University of Texas Rio Grande Valley
ScholarWorks @ UTRGV

Theses and Dissertations

5-2021

Exploration of Antimicrobial and Cell Proliferation Properties of Nanofibers Incorporating Nopal (*O. cochenillifera*) Extract

Cristobal Rodriguez
The University of Texas Rio Grande Valley

Follow this and additional works at: https://scholarworks.utrgv.edu/etd

 Part of the Biology Commons, and the Nanoscience and Nanotechnology Commons

Recommended Citation

Rodriguez, Cristobal, "Exploration of Antimicrobial and Cell Proliferation Properties of Nanofibers Incorporating Nopal (*O. cochenillifera*) Extract" (2021). *Theses and Dissertations*. 757.
https://scholarworks.utrgv.edu/etd/757

This Thesis is brought to you for free and open access by ScholarWorks @ UTRGV. It has been accepted for inclusion in Theses and Dissertations by an authorized administrator of ScholarWorks @ UTRGV. For more information, please contact justin.white@utrgv.edu, william.flores01@utrgv.edu.

EXPLORATION OF ANTIMICROBIAL AND CELL PROLIFERATION PROPERTIES OF NANOFIBERS INCORPORATING NOPAL (*O. COCHENILLIFERA*) EXTRACT

A Thesis

by

CRISTOBAL RODRIGUEZ

Submitted to the Graduate College of
The University of Texas Rio Grande Valley
In partial fulfillment of the requirements for the degree of

MASTER OF SCIENCE

May 2021

Major Subject: Biology

EXPLORATION OF ANTIMICROBIAL AND CELL PROLIFERATION PROPERTIES OF NANOFIBERS INCORPORATING NOPAL (*O. COCHENILLIFERA*) EXTRACT

A Thesis
by
CRISTOBAL RODRIGUEZ

COMMITTEE MEMBERS

Dr. Robert Gilkerson
Chair of Committee

Dr. Karen Lozano
Committee Member

Dr. Megan Keniry
Committee Member

Dr. Andrew McDonald
Committee Member

May 2021

Copyright 2021 Cristobal Rodriguez

All Rights Reserved

ABSTRACT

Rodriguez, Cristobal, Exploration of Antimicrobial and Cell Proliferation Properties of Nanofibers Incorporating Nopal (*O. cochenillifera*) Extract. Master of Science (MS), May, 2021, 43 pp., 2 tables, 16 figures, 90 references, 90 titles.

This study focused on the fabrication of Forcespinning® nanofibers composed of *Opuntia cochenillifera*, 'nopal', mucilage (N) extract, chitosan (CH), and pullulan (PL) (N/CH/PL) were developed with an optimum fiber average diameter of 406±127 nm, and studied for their ability to sustain adhesion and proliferation of mouse embryonic fibroblast (NIH 3T3) cells. After a 6-day incubation period, N/CH/PL nanofibers displayed robust cell proliferation, while also exhibiting inhibitory properties through an N extract dip-coating process against gram-negative bacteria *Escherichia coli* in a 24 h bacterial growth study. A demonstration of integrated natural bioactive compounds with combined biodegradable polymers, provide an enhanced environment for cell growth, leading to a possible natural alternative for wound dressing applications.

DEDICATION

This master's study comes from the support and care of my friends and family. To my parents Aleida and Daniel Rodriguez, that have continuously displayed their pride towards our Mexican heritage, which has inspired me to apply within all my work. This could not have been possible without their care, patience, and sacrifice.

ACKNOWLEDGMENTS

I am honored to have been guided and instructed under Dr. Robert Gilkerson, who had given me the opportunity to conduct research ever since high school; where I was first introduced to confocal microscopy. Thank you for all the advice, funding, research skills, and aid in my thesis. Also, thank you for the constant support of my work and the value of importance that was always placed into it. Thank you to Dr. Karen Lozano for allowing me to participate in the Partnership for Research and Education in Material Science (PREM) program, the continued funding, and for the constant advice and encouragement given. I will also be grateful to my committee members Dr. Megan Keniry and Dr. Andrew McDonald for their knowledge that they have imparted into my thesis work.

I am thankful also for my fellow research lab partners Iraselia, Alejandra, Fariha, Patrick, Shayna, and Cesar who form a wonderful team in Dr. Gilkerson's lab. Also, thank you Dr. Victoria Padilla, Astrid Rodriguez, and my fellow members from PREM for all the help around the Nano lab.

TABLE OF CONTENTS

LIST OF TABLES

Page

LIST OF FIGURES

Page

CHAPTER 1

INTRODUCTION

Statement of the Problem

Emerging nanofiber technologies hold potential for a range of biomedical applications. The ability of nanofibers to simulate the extracellular matrix (ECM) in biological tissues via a porous three-dimensional surface area motivates the exploration of nanofibers for wound healing applications (Boyle *et al*., 2019; Cremar *et al*., 2018). Standard techniques, such as electrospinning allow the production of nanofibers from a variety of polymers, but are limited in the yield of nanofibers produced (Akia *et al*., 2019; Xu *et al.*, 2014). Conversely, Forcespinning® (FS) allows the mass production of nanofibers by using centrifugal force to generate a homogenous polymer solution (Padron *et al*., 2013). This method allows production of composite nanofibers with robust yield from a range of polymeric compositions (Akia *et al*., 2018; Padilla-Gainza *et al*., 2019; Padron *et al*., 2013). Previously, citric acid (CA) was used for esterification mediated fiber crosslinking (Shi *et al*., 2009) in combination with chitosan (CH) and pullulan (PL) to develop biocompatible ternary composite nanofibers to support cell growth (Xu *et al*., 2014), suggesting that FS-produced nanofibers may have promise for wound healing applications. Here, we explore the production of FS nanofibers incorporating cactus extract from *O. cochenillifera*, native to much of the Americas, including Mexico and Texas.

Incorporation of bioactive plant compounds to polymeric materials may improve wound healing capability. In tissue remodeling, complications to wound healing are caused by multiple factors such as prolonged inflammatory response due to an increase in free radicals, and the presence of pathogenic bacteria (Guo & DiPietro, 2010; Lobo, Patil, & Chandra, 2010). Plant components may have antioxidant properties to inhibit or scavenge reactive oxygen species (ROS), while phenolic acids may prevent bacterial growth (Abbas *et al*., 2017; Khemiri, Hedi, Zouaoui, Gdara, & Bitri, 2019; Lobo, Patil, & Chandra, 2010). Plant-based extracts may be useful as bioactive components of nanofiber matrices for enhanced cell proliferation and improved wound healing (Khemiri *et al*., 2019). Many naturally derived plant-based components, traditionally used as homeopathic medicines, have putative antioxidant, anti-inflammatory, and antibacterial properties (Blando, *et al*., 2009; El-Mostafa *et al*., 2014; Lee *et al*., 2002; Osuna-Martinez *et al*., 2014).

Among the family Cactaceae, species within the genus *Opuntia* are widely distributed throughout North and South America. Due to the domestication of several species in the genus, expanded distributions of several domesticates resulted in novel hybridization and speciation events (Kiesling, 2009; Majure & Puente, 2014). In addition, artificial selection of *Opuntia* gave rise to various modified forms without altering their success in a wide range of environmental conditions (Majure & Puente, 2014). *Opuntia* spp. are able to survive both extreme cold and heat as well as dry conditions, and exhibit strong water retention capabilities (Sepulveda et al., 2007).

Opuntia cochenillifera (L.) Mill., known colloquially as ‘nopal,’ has been used as a homeopathic folk medicine, as well as for agricultural purposes due to its enriched mineral composition (Sepulveda *et al*., 2007; Saenz, Sepulveda, & Matsuhiro, 2004). Cacti may also

confer naturally-derived anti-oxidant and anti-inflammatory properties for wound healing applications (Chen *et al*., 2011; Santos *et al*., 2017). Cactus mucilage has previously been incorporated into nanofibers produced by electrospinning (Pais, 2011; Thomas & Alcantar, 2017), but the ability of cells to grow on these fibers has not been investigated.

Statement of Purpose

The ability of mammalian cells to proliferate on nanofiber matrices suggests potential medical applications; however, the interaction of nanofibers and mammalian cells is still not fully understood. This research explores 1) the fabrication of FS-produced ternary composite nanofibers based on chitosan (CH), pullulan (PL), and *O. cochenillifera*, nopal, mucilage (N) extract, and 2) the ability of cultured cells to growth on these fibers due to a small fiber diameter and the incorporation of bioactive compounds. We hypothesize that a nanofibrous material could improve cell viability through incorporation of plant based bioactive compounds allowing for cell adhesion and proliferation. This nanofiber environment, resembling the extracellular matrix (ECM) in surface area and high aspect ratio, may facilitate cell proliferation and migration with potential for a variety of physiological applications (Xu *et al*., 2014). In this study, N/CH/PL composite nanofibers incorporating varying concentrations of N extract and binary CH/PL composites were characterized via scanning electron microscopy (SEM), a thermogravimetric analysis (TGA), and Fourier-transform infrared spectroscopy (FT-IR), followed by exploring the effect of incorporation of bioactive compounds on cell adhesion, proliferation, and cytotoxicity through cell viability analysis as compared with control composite nanofibers without N extract. Our data suggests that FS-produced of nanofibers incorporating naturally-derived bioactive extracts have full structural integrity and antibacterial properties, with the ability to support mammalian cell growth. This motivates future work exploring the interaction of these fibers with mammalian cells for potential improved wound healing applications.

CHAPTER II

REVIEW OF LITERATURE

Advancements in Nano-scale Material

Advancements in nano-scale material have included protein binding and impregnation in drug delivery systems to improve wound healing (Hajialyani *et al*., 2018). Considered characteristics over material sustainability have been described with a possible solubility, pH, and thermal stability of an incorporated protein or chemical cue markers (Jenkins & Little, 2019). Cell adhesion molecules (CAMs), such as cadherin or integrin, confer the ability of cells to adhere onto fibrous or connective tissue. The extracellular matrix (ECM) functions as a fibrous environment for support (Sherwood, 2016). Cells are suspended in this fluid system allowing the exchange of nutrients, waste, and fibroblast collagen secretion. The successful incorporation of silver nanoparticles was previously incorporated in chitosan-based nanofibers, with antibacterial effects against microbes and other pathogens (Cremar *et al*., 2018). Surface-integrated zinc oxide nanoparticles was combined in poly(D, L-lactic acid) (PDLLA) and poly(3-hydroxybutyrate) (PHB) for growth of pre-osteoblast cells (Padilla-Gainza *et al*., 2020). In Boyle *et al*. (2019), found that reduced levels of inflammatory chemokines, monocyte chemoattractant 1 (MCP-1), and interleukin 8 (IL-8) were present in recessive dystrophic epidermolysis bullosa (RDEB)-squamous cell carcinoma (SCC) conditioned media within the presence of ternary composite nanofibers; while also presenting a low SCC cell migration. Ternary composite nanofibers were shown to be effective in the removal of inflammatory chemokines, which could

improve wound treatment within RDEB patients. Composite nanofibers displays a small fiber diameter range from ~300 to 600 nm in average size (Xu *et al.,* 2015). Implying the variation in testing the physical characteristics and incorporation in nanomaterials needed to acquire the desired properties in improving cell adhesion and proliferation.

Wound Healing and Complications

Wound Healing

The skin is one of the major forms of defense against physical damage and exterior pathogens. Through the epidermal, dermal, and subcutaneous layers, pathogenic invasion is combatted by both innate and adaptive immune responses that targets foreign entities (Sherwood, 2016) (Fig. 1). Through skin lesions, a rapid immune response is initiated by invading bacteria found on the skin's surface surrounding the wound area, where they meet phagocytic cells or inactivating molecules with/ Toll-like receptors (TLRs) responding to Pathogen-associated molecular patterns (PAMPs) and danger-associated molecular patterns (DAMs) (Macleod & Mansbridge, 2014). Inflammation then occurs through the increased flow of blood containing phagocytic cells that removed damaged tissue and other foreign anomalies, while macrophages may mediate an anti-inflammatory response through the mediation of mi21- (Macleod & Mansbridge, 2014). This further allows the migration of fibroblasts cells, which initiate the production of collagen and wound closure with connective tissue or neighboring cells (Sherwood, 2016).

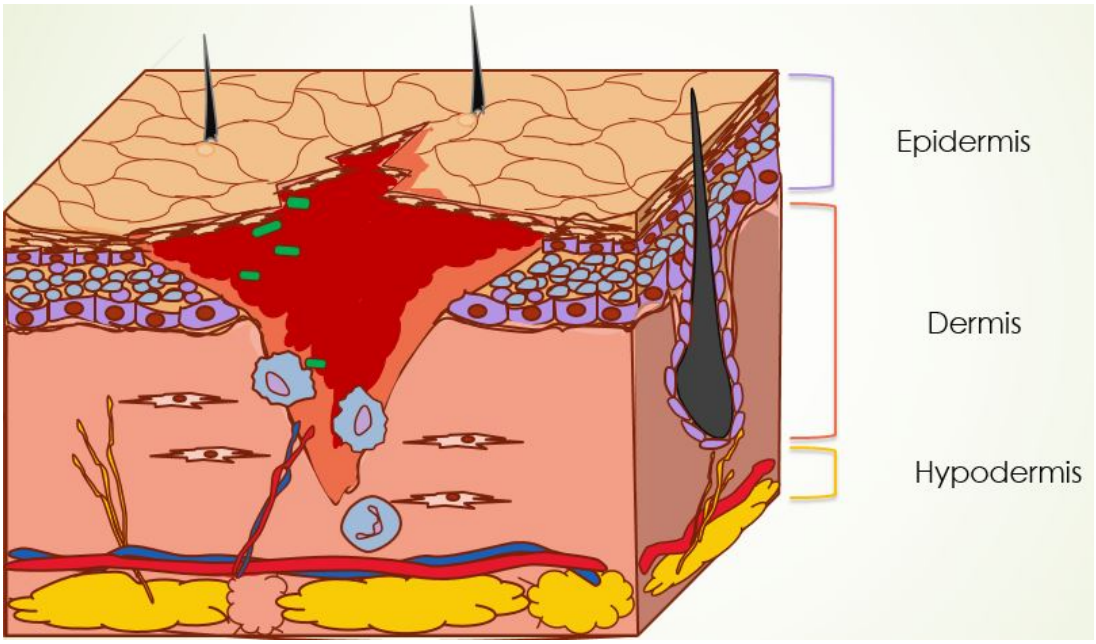

Figure 1. Wound Model: Upon initial damage, and innate immune response is activated through phagocytes, white blood cells, and migrating fibroblasts for wound repair and closure.

Wound Complications

Wound healing complications include excessive immune response and inflammation, as well as potential bacterial infection (Guo & Di Pietro, 2010). These complications include tissue damage and inflammatory response, which lead to the production of cytokines, free oxidative radicals, and other inflammatory signaling molecules associated with prevalent conditions, including diabetes mellitus, cardiovascular disease, and aging (Lobo *et al*., 2010; Sen, 2019). Complications in diabetic patients include elevated signaling of inflammatory cytokines tumor necrosis factor-alpha (TNF-α) and interleukin-6 (IL-6) (DeClue & Shornick, 2015); Tanaka, Narazaki, Kishimoto, 2014), which reduce cell viability due to their negative effects within the immune response in wounds (Xu, Zhang, & Graves, 2013). Upon release by macrophages, TNF-α binds to two membrane receptors: tumor necrosis factor receptor 1 (TNFR1) and tumor

necrosis factor receptor 2 (TNFR2); also known as TNFR1 (p55) and TNFR2 (p75), causing an inflammatory response (Harth & Rosen, 2009; Parameswaran & Patial, 2010) and activation of fas associated death domain (FADD) and caspases leading to apoptosis (Chau, Chen, Wan, DeGregori, Wang, 2004). Prolonged exposure of TNF-α and IL-6 may lead to complications seen through minor lesions, which may develop into a chronic state due to improper wound treatment placing the patient susceptible to infections.

Plant Innate Immunity and Phytochemical Content

Plant Innate Immunity

The evolutionary development of plants has allowed them to sustain innate immune response to pathogens. Cell membrane Pattern-Recognition Receptors (PRR) and cytoplasmic receptors enable the plant cell's ability to signal targeted pathogens (Kushalappa, Yogendra, & Karre, 2016). In the activation and recognition of pathogens, the pathogen/microbe-associated molecular patterns (PAMPs or MAMPs) initiate the PAMP-triggered immunity (PTI) activation through PRRs. This defensive system further reverses any reaction caused by the pathogen through the plant's nucleotide-binding-leucine-rich repeat (NB-LRR), targeting the conserved domains of microbes (Boller & He, 2009). Viral infection NB-LRR leads to activation of viral effector-triggered immunity (ETI), while intracellular immune resistance proteins (R) help in detecting secreted viral effectors (Calil & Fontes, 2017).

Plant Phytochemical Content

Plants have a high complex carbohydrate content, with simple sugars (Rodriguez-Gonzalez *et al*., 2014; Hernandez-Carillo, Gomez-Cuaspud, & Martinez-Suarez 2017; Sepulveda et al., 2007; Thomas & Alcantar, 2017). For example, *Opuntia cochenillifera* (L.) Mill., known as 'nopal', has been used for agricultural purposes as a consumed food source due to its high

supplemental mineral content in Ca, K, Mg, vitamin E and C (Saenz, Sepulveda, & Matsuhiro, 2004; Sepulveda *et al*., 2007). Further *Opuntia* mucilage analysis identified the presence of carbohydrates such as L-rhamnose, D-galactose, L-arabinose, and uronic acids (Bayar *et al*., 2016; Guadarrama-Lezama, Castaño, Velazquez, Carillo-Navas, & Alvarez-Ramirez, 2018; Monrroy, Garcia, Rios, Renan-Garcia, 2017; Ondarza, 2016; Olivarez-Perez, Toxqui-Lopez, & Padilla-Velasco, 2012; Park, 2002). Cactus mucilage has also traditionally been used for folk medicinal purposes due to anti-oxidative and anti-inflammatory properties with potential wound healing capabilities (Chen *et al*., 2011; Da Cruz Filho *et al*., 2019; Del Socorro Santos Diaz *et al*., 2017; Keen & Hassan, 2016).

Plant Based Materials

The incorporation of physiochemical compounds has been described in different applications of plant-based materials through fiber electrospinning techniques, as seen in Table 1. Plant materials are utilized for phytochemical content found in seeds, flowers, leaves, and even roots. Smart materials may mimic plant behavior for sensing and material morphology changes (Lunni *et al*., 2020). From a mucilage plant extract, multiple physiochemical compounds are present with an unaltered composition, where prevention in protein and molecule disruption could be exhibited through a simplified extraction. Incorporation of naturally-derived bioactive compounds through the FS technique (Fig. 2) would enable the production of fibers and the potential to restore or improve a wound healing (Padron *et al*., 2013).

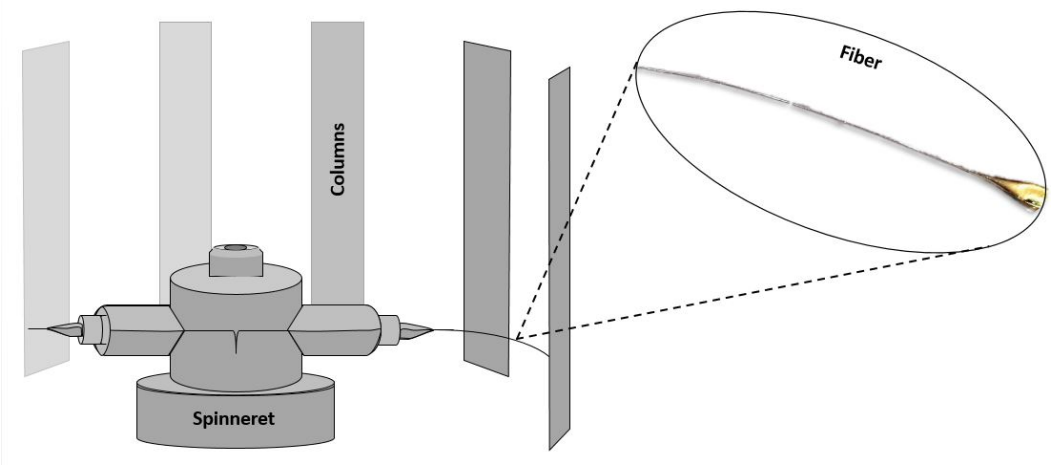

Figure 2. Diagram of Forcespinning®, with surrounding columns, producing dried fibers from a homogenous polymer solution.

Table 1. Plant based materials and their applications.

Plant Species	Part	Application	Material	Reference
Prosopis juliflora	Stalks	Reinforced polymers composite, Papermaking, Plastics and textile industry	Fibers	Mohammed *et al*. (2019)
Medicago stiva	Alfalfa leaf	Wound healing	Spun Nanofibers	Ahn *et al*. (2019)
Hyptis suaveolens, *Linum usitatissimum*, *Triumfetta semitriloba*	Chan Seed, Linaza Seed, Mezote Stem (mucilage)	Tissue engineering	Electrospun Nanofibers	Urena-Saborio *et al*. (2018)
Alyssum lepidium	*Alyssum* seed (mucilage)	Water filtration and drug delivery	Electrospun Nanofibers	Golkar et al. (2018)
Musa paradisiaca	Mature plantain	Reinforced polymers	Nanocomposite Films	Pelissari *et al*. (2017)
Opuntia ficus-indica	Nopal pads	Reinforced polymers	Nanowhiskers	Vieyra *et al*. (2015)
Maize (Corn)	Zein protein	Wound dressing	Electrospun Nanofibers	Dashdorj *et al*. (2015)
Aloe vera	Leaf	Tissue engineering	Electrospun Nanofibers	Suganya *et al*. (2014)
Astragalus spp.	Gum tragacanth	Wound dressing	Electrospun Nanofibers	Ranjbar-Mohammadi *et al*. (2013)
Aloe vera	Leaf	Wound healing and drug delivery	Hydrogel films	Pereira *et al*. (2013)

CHAPTER III

METHODOLOGY AND FINDINGS

Materials and Methods

Materials

Low molecular weight (50-190 kg·mol-1, based on viscosity) chitosan (CH), citric acid (CA) were purchased from Sigma-Aldrich®, and pullulan (PL) (P0978) was purchased from Tokyo Chemical Industry Co. Ltd. (TCI). Deionized water (DI) (18.20 MΩcm) filtered through Barnstead MicroPure ST® (Thermo Fisher Scientific), and 70% Denatured Ethyl Alcohol (Fisherbrand™). Dulbecco's Modified Eagle Medium (DMEM (1X)) (Gibco™) was obtained from Thermo Fisher Scientific, and phosphate-buffered saline (10X PBS solution) was purchased from Fisher-Bioreagents™. Resazurin (sodium salt) obtained from ACROS (Organics™).

Mucilage Extraction

Cladode was collected from *O. cochenillifera* plant (originally from Matehuala, San Luis Potosi, Mexico). Leaves were removed with a sterile blade leaving a bare cladode, which was then rinsed with DI water (18.20 MΩcm) followed by sterilizing with 70% denatured ethyl alcohol. Cladode was then diced and crushed in a mortar, where crude *O. cochenillifera*, 'nopal', mucilage (N) extract was obtained. A 5 mL plastic syringe was used to collect N extract in order to transfer into a 15 mL centrifuge tube, which was centrifuged (CompactStar CS4, VWR®) for 10 min at 6000 rpm to further separate mucilage extract. N extract supernatant was then collected and filtered using a 0.22 μm size syringe filter.

Solution Preparation

Solutions were prepared by dissolving 2.4 wt% CH into CA solution (3.2 wt% CA in 10 mL DI water) and left stirring overnight. PL (14.4 wt%) was then added into the CA/CH prepared solution, left continuously stirring for 2 h and vortexed until fully dissolved. Similar polymer concentrations were used at different increasing N extract presence. Specifically, N extract/DI water volume ratios of 1:9 (V/V) combined with CH/PL to produce N1/CH/PL (N1) composites, N extract/DI water 5:5 (V/V) for N50/CH/PL (N50), and a complete N extract volume (replacing DI water) was used for CH/PL solution to produce N100/CH/PL (N100).

Nanofiber Production

Nanofiber samples were spun at low (33-50%) relative humidity levels at 7000 rpm via FS on a Cyclone™ L-1000M (FibeRio Technology, Corp.) equipped with a cylindrical spinneret. This system allowed for the facile production of fine fibers (Padron *et al*., 2013). To produce fibers, 2 mL of prepared polymer solution were injected with a 3 mL plastic syringe and released as fine solution jets from screwed syringe needles at the two ends of the spinneret, which were allowed to deposit as dried fibers on 10 collector columns surrounding the spinneret at an 8-inch distance. A collector aluminum covered frame was used for the collection of nanofibers, followed by a crosslinking heat treatment process at ~140 ºC for 1 hour (Xu *et al*., 2014).

Nanofiber Characterization

Binary CH/PL (control) and nopal-containing N/CH/PL nanofiber membranes were cut into ~5 mm x 5 mm mats, sputter-coated with gold, and imaged using a scanning electron microscope SEM (Carl Zeiss, SigmaVP). ImageJ 1.50i software was then utilized to determine an average fiber diameter distribution, with 300 fibers measured per sample. A thermogravimetric analysis (TGA) (TA® Instrumentation SDT-Q600 Simultaneous TGA/DSC)

was conducted to analyze concentration and thermal degradation of components. Samples weighing 10 mg, were heated on a platinum pan from room temperature to 600 ºC at a heating rate of 20 ºC min^{-1} under airflow. Fourier transform infrared spectroscopy (FTIR) (VERTEX 70v FTIR Spectrometer, Bruker®) analysis was conducted in transmittance mode (4000-400 cm^{-1}).

Nanofiber Water Absorption Capacity

Water absorption analysis was conducted by submerging nanofibers samples in deionized water for ~1 h. Samples were air-dried for 5 min, and their final weight (W_f) was then subtracted from the initial weight (W_i) to calculate a water absorption capacity as depicted in Equation 1.

$$\text{Water absorption capacity (\%)} = [(W_f - W_i)/W_i] \times 100 \qquad \textit{Equation 1}$$

Dynamic Mechanical Analysis (DMA)

For the mechanical performance of DN100 samples, a DMA in a tensile mode was conducted utilizing a DMA 242 E *Artemis* (NETZSCH®, Germany). Samples with dimensions of 5 x 2 x 1 mm^3 were partially hydrated, and fine-grit sandpaper slips were placed at the two ends of the fiber samples to clamp them in the jaws of the sample holder; to further avoid sample slippage during the test. The analysis was conducted at a frequency of 1 Hz, with a strain amplitude of 0.16%, a static force of 0.3 newton (s) (N), and a temperature range of 23 °C to 40 ºC at a 2.0 (K/min) rate under an ambient air environment.

Mucilage Dip-coating Process

For the process of dip-coating, N100 nanofiber membranes (DN100) were cut into disk shapes of 1 cm in diameter and submerged in 1 mL N extract for 1 h. After 1 h, DN100 samples were removed and air-dried. Samples were then covered and sealed with parafilm in a small petri dish, and refrigerated at 4 ºC for 24 h for preservation and drying.

Antibacterial Study

Bacteria growth of gram-negative *Escherichia coli* (*E. coli*) (ATCC 8739) resistance or susceptibility response was determined by utilizing the Kirby-Bauer disk diffusing analysis (Hudzicki, 2009; Talaro & Chess, 2015). 100 µL of inoculated *E. coli* cell suspension, were spread onto Mueller-Hinton agar plates. Nanofiber samples were cut into disk shapes of 1 cm in diameter, and DN100 nanofibers were placed individually onto spread *E. coli* cultures and incubated at 37 ºC for 24 h. After 24 h, the inhibition zones were observed and measured.

Mammalian Cell Culture

Mouse embryonic fibroblasts (NIH 3T3) cells (provided by Eric Schon, Columbia University) were cultured in Dulbecco's Modified Eagle Medium (DMEM) with 10% fetal bovine serum (FBS), 100 IU mL^{-1} penicillin, and 100µg mL^{-1} streptomycin, and incubated at 37 ºC in a 5 % CO_2 environment.

Confocal Microscopy and Sample Preparation

CH/PL, N1, N50, N100, and DN100 nanofiber samples were cut ~7 mm x 7 mm, and sterilized under UV-light for 10 min. Samples were then hydrated with medium and seeded with 1.2 x 10^5 NIH 3T3 cells in a 6-well culture plate, which was incubated at 37 ºC in a 5 % CO_2 environment over the course of 2, 4, and 6 days. After incubation, samples were lifted with glass coverslips and placed in a new 6-well plate. Samples were treated for 20 min at 37 ºC with 40 nM MitoTracker Red® (MTR) CMXRos, followed by both medium and 1xPBS washes. Samples were then fixed with 4 % formaldehyde for 30 min, followed by 300 nM 4', 6-diamino-2-phenylindole (DAPI) staining. After several 1xPBS washes, samples were prepared and mounted with 50% glycerol for imaging using an Olympus® FV10i confocal laser-scanning microscope.

SEM Cell Morphology and Adhesion Analysis

To further assess the morphology and adhesion of NIH 3T3 cells, CH/PL and N100 nanofibers were cut ~7 mm x 7 mm, and sterilized under UV-light for 10 min. Samples were then hydrated with medium and seeded with 1 x 10^4 NIH 3T3 cells in a 24-well culture plate, which was incubated at 37 ºC in a 5% CO_2 environment over the course of 6 days. After incubation, samples were lifted and placed in a new dish then washed twice with 1xPBS. Samples were then fixed for 1 h, washed with 1xPBS, followed by dehydration with 100% ethanol for 10 min, and left overnight for full drying in a parafilm sealed small petri dish at 4 ºC. Once dried, samples were sputtered coated with gold and analyzed through an SEM. The method was modified from Dashdorj *et al*., (2015).

Cell Viability

Resazurin cell viability test was conducted in order to evaluate the metabolic activity of NIH 3T3 cells. CH/PL and N100 nanofiber samples were cut ~7 mm x 7 mm, sterilized under UV-light for 10 min, then glued down onto the bottom of the culture plate for a direct exposure. A cell density of 1 x 10^4 NIH 3T3 cells were seeded in a 24-well plate, where a positive control was compared between CH/PL and N100 samples in a 2, 4, and 6 day incubation period at 37 ºC in a 5% CO_2 environment. Samples were treated with 300 µL of prepared Resazurin solution (0.01 wt% in 10 mL DI water) and incubated for 4 h for reaction. After incubation, 300 µL of the reaction were loaded into a 96-well plate and read in a microplate reader (BioRad®) at 570 nm. Protocol was modified from Saenz *et al*. (2016).

Cell-nanofiber Depth Analysis

To determine 3T3 cell proliferation and migration within nanofibers, a depth analysis was conducted. A cell density of 1.2 x 10^5 3T3 cells were seeded onto CH/PL and N100 samples for a 14-day incubation at 37 ºC in a 5% CO_2 environment. Cell culture media was changed and

replenished every 4 days. After incubation, samples were lifted onto glass coverslips and placed in a new 6-well plate. Samples were then treated with MTR and DAPI, as above, followed by fixing and prepping for mounting for confocal microscopy.

Statistical Analysis

In all experimental studies, samples were conducted in triplicate. A t-test was performed for mean ± SD values through GraphPad Software Inc., followed by a statistical analysis between mean sample variance through one-way ANOVA/Post-hoc Tukey's test analysis, where a significant difference was based on a $p\text{-value} < 0.05$.

Results and Discussion

Polymers

Chitosan is a cationic linear polysaccharide (1-4)-2-amino-2-deoxy-β-D-glucan natural polymer (Fig. 3(a)), with antimicrobial, fibrous, and encapsulation capabilities for drug delivery systems (Xu *et al*., 2015). This natural biocompatible and biodegradable polymer is able to interact with multiple enzymatic and cellular targeting functions (Teixeira *et al*., 2017). As CH is insoluble in water, an acidic aqueous solution was required for a full polymer solubility and subsequent use in-multiple polymer combinations. Pullulan a natural linear exopolysaccharide (Fig. 3(b)), described with a α-(1-6) maltotriose unit where its alpha-linkage provides a physical ability to be flexible and water soluble (Coltelli *et al*., 2020).

Nanofiber Production

In order to fabricate nanofibers containing *O. cochenillifera* (Fig. 4(a)) (N) extract, pullulan (PL) was used due to its biodegradable and fiber integrity, while citric acid (CA) and chitosan (CH) were used to allow a crosslinking reaction to promote water stability as previously shown (Xu *et al*., 2014). Using the FS method, N extract-based nanofibers were produced at

varying concentrations as N1, N50, and N100 (Fig. 4(b)). SEM micrographs in Figure 5(a-d), show long continuous fiber structure obtained for all samples at different concentrations of N extract with some bead formation. Figure 5(e-h) depict a one-way ANOVA past-hoc Tukey statistical analysis with a significant difference (***$p < 0.001$) between samples, where CH/PL displayed an average fiber diameter of 260 nm with a standard deviation of 82 nm with no significant difference ($p > 0.05$) with N1/CH/PL with an average fiber diameter of 251±77 nm, while N50/CH/PL and N100/CH/PL show 341±112 nm and 406±127 nm, respectively. The range in fiber diameter could be attributed to the concentration of N extract, where an increase in viscosity of solution due to high mucilage concentration used was shown (Cardenas, Higuera-Ciapara, & Goycoolea, 1997; De J. Cano-Barrita & Leon-Martinez, 2016; Monrroy, Garcia, Rios, Renan-Garcia, 2017; Obregon *et al*., 2016), potentially influencing the average nanofiber diameter between samples.

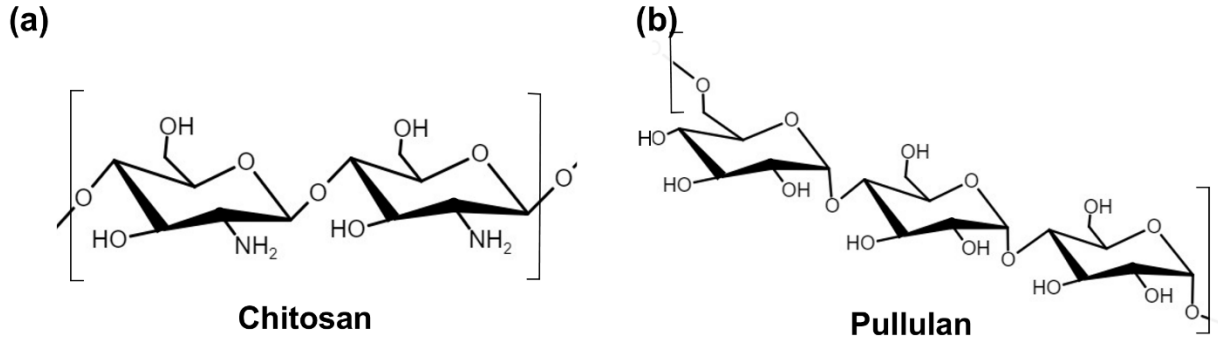

Figure 3. Structure of chitosan (a) and pullulan (b) are displayed provided by Marvin JS TCI© drawing tool program.

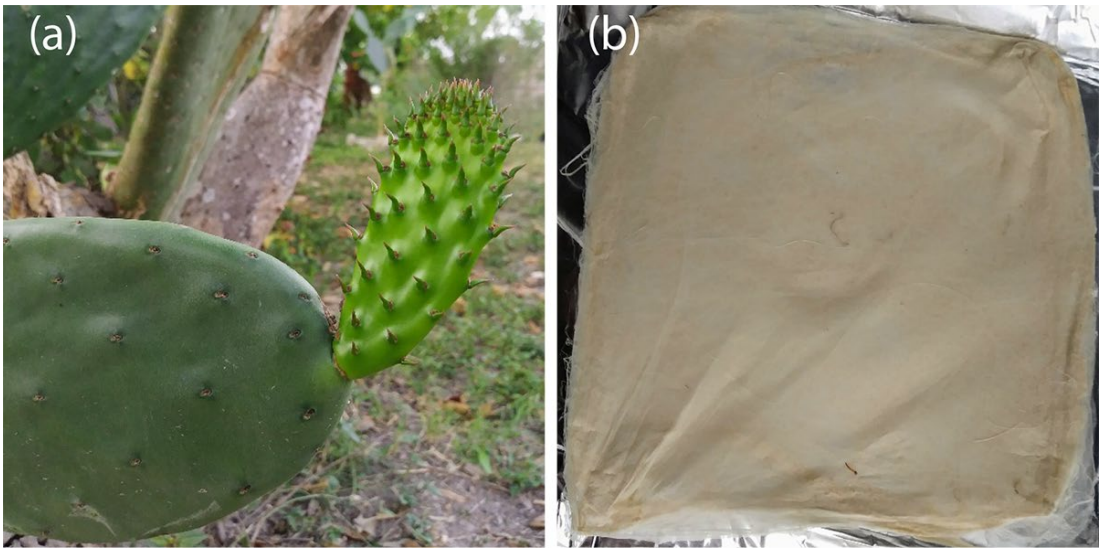

Figure 4. *O. cochenillifera* (a) and FS N/CH/PL nanofiber 5 x 5 inch mats (b) are displayed.

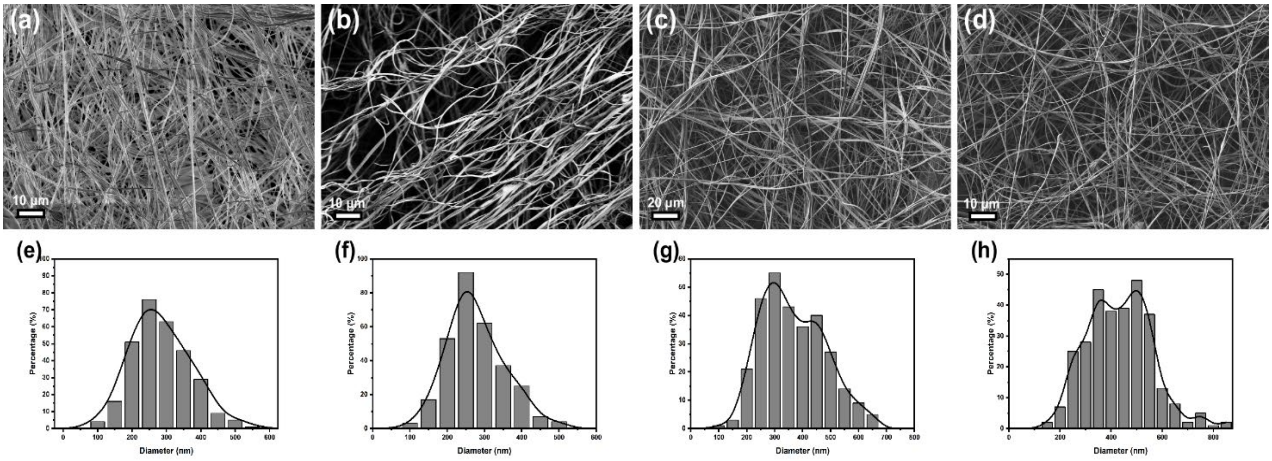

Figure 5. SEM Analysis of Nanofiber morphology and Fiber Diameter Distribution: Nanofiber morphology for CH/PL (a), N1 (b), N50 (c), and N100 (d) nanofibers is shown. Graphs are shown with nanofiber diameter distribution of CH/PL (e), N1/CH/PL (f), N50/CH/PL (g), and N100/CH/PL (h). Sample size: n= 300. One-way ANOVA post-hoc Tukey's test exhibited a significant difference between samples ($p < 0.001$), while a non-significant difference between CH/PL (e) and N1/CH/PL (f) ($p > 0.05$) is shown.

Thermal Degradation Analysis

The degradation patterns of nanofibers with different concentrations of N extract are shown in Figure 6(A). Systems presented an initial weight loss at ~100 ºC, corresponding to water evaporation; specifically, in the range of 50 to 180 °C the physically adsorbed water was of 10.3, 9.03, 9.03, 9.07, and 11.6 % for CH/PL, N1/CH/PL, N50/CH/PL, N100/CH/PL, and DN100 respectively. On the other hand, within the second degradation stage, when 5% of polymeric material has degraded a slight decrease in the thermal stability was observed with the increase of the N extract concentration. The DN100 degradation pattern presented similarities with the nopal mucilage extract thermogram reported by Lopez-Garcia *et al*. (2017), where the degradation temperature (Td) was 220 °C, slightly less than pullulan and chitosan. However, it was observed that the system degradation profiles changed with temperature; at ~300 °C the N extract systems presented a greater thermal stability with a pronounced effect on the DN100, possibly due to the reaction of the remaining components within the systems, producing a strong network (Nady & Kandil, 2018). In addition, these last stages could be related to the portion of crosslinked components that originated with the heat treatment carried out in the manufacturing stage of the systems (Zhuang, Zhi, Du, & Yuan, 2020). In Figure 6(B), the exothermic reaction peaks related to the degradation stages are clearly observed, an increase in the enthalpy of the reaction is observed for the last stage of degradation; 294, 2600, 3375, 4277, and 5423 J/g for CH/PL, N1/CH/PL, N50/CH/PL, N100/CH/PL, and DN100 respectively. An increase in thermal stability is exhibited in composite nanofibers undergoing a crosslinking heat treatment process at 140 ºC, as through the initial degradation patterns.

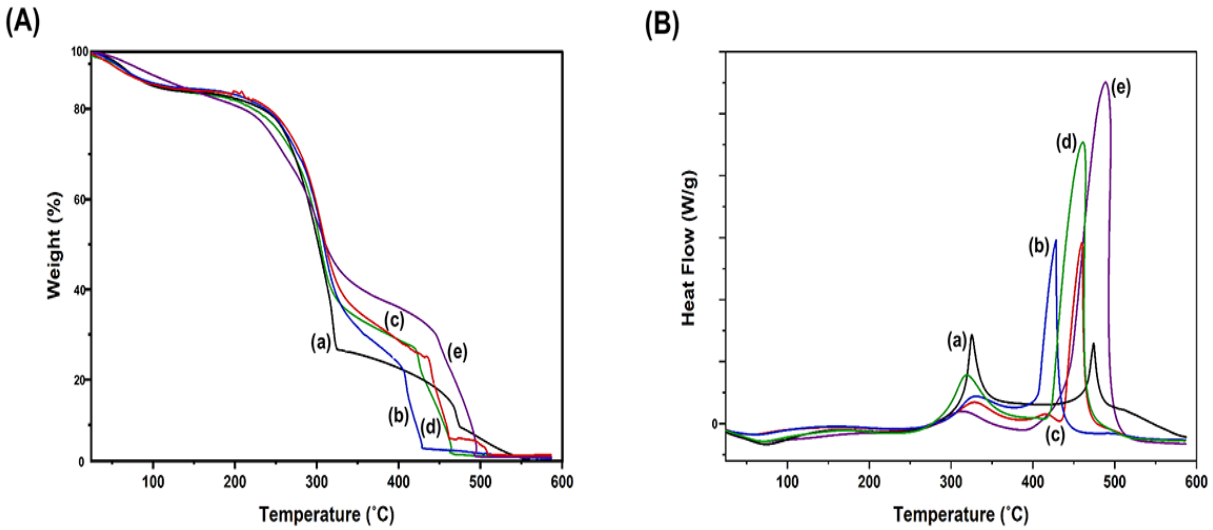

Figure 6. TGA analysis on nanofibers: TGA weight (%) loss (A) and heat flow (B) of nanofiber samples CH/PL (a), N1 (b), N50 (c), N100 (d), and DN100 (e).

FTIR Analysis

Figure 7 shows the FTIR spectrums of the CH/PL, N1/CH/PL, N50/CH/PL, N100/CH/PL, and dry N extract in order to further elucidate the presence of N extract components at an increasing concentration. As can be seen in all the spectra, the characteristic bands of polysaccharides are identified through different functional groups such as carboxylic acid, carboxylate, ether, amide, and alcohol groups. The broad band in the interval 3500-3100 cm^{-1} corresponds to O-H stretching from alcohol and carboxylic acid-OH groups involved in hydrogen-bond formation between polysaccharide chains and water molecules (Monrroy *et al*., 2017); similar behavior observed in all the systems. The free carboxyl group promotes the water absorption capabilities, which is a defining property of these systems (Cardenas *et al*., 1997; Rodriguez-Gonzalez *et al*., 2014). Bands around 2900 cm^{-1} related to the vibrations of CH and CH_2 groups as previously described (Karim *et la*., 2009; Rodriguez-Gonzalez *et al.*, 2014; Xu, Weng, Gilkerson, Materon, Lozano, 2015). However, this vibrational band has also been assigned to the methoxy group in the nopal extract (Guadarrama-Lezama *et al*., 2018). A

transmittance peak at ~1718 cm^{-1}, relates to a C=O stretching vibration from carboxylic groups which appears with more intensity as the nopal concentration increases. Two bands are shown at ~1640 cm^{-1} and ~1585 cm^{-1}, which correspond to the N–H bending vibration of primary amines (Yasmeen *et al*., 2016) or/and C=O vibration of amino acid (Hernandez-Carillo, Gomez-Cuaspud, & Martinez-Suarez, 2017; Olivarez-Perez, Toxqui-Lopez, & Padilla-Velasco, 2012). The CH^2 bending was confirmed by the presence of bands around 1450 cm^{-1}. A peak at 1240 cm^{-1}, can be based on C-O stretching from hydroxyl groups. Finally, the transmittance band at 1153 cm^{-1} and 1045 cm^{-1} can be attributed to asymmetric stretching of the C-O-C bridge and C-O vibrations, respectively (Rodriguez-Gonzalez *et al.,* 2014). Through the combination of natural polymers and N extract content, the presence of polysaccharides remains while exhibiting no chemical alteration after the crosslinking process.

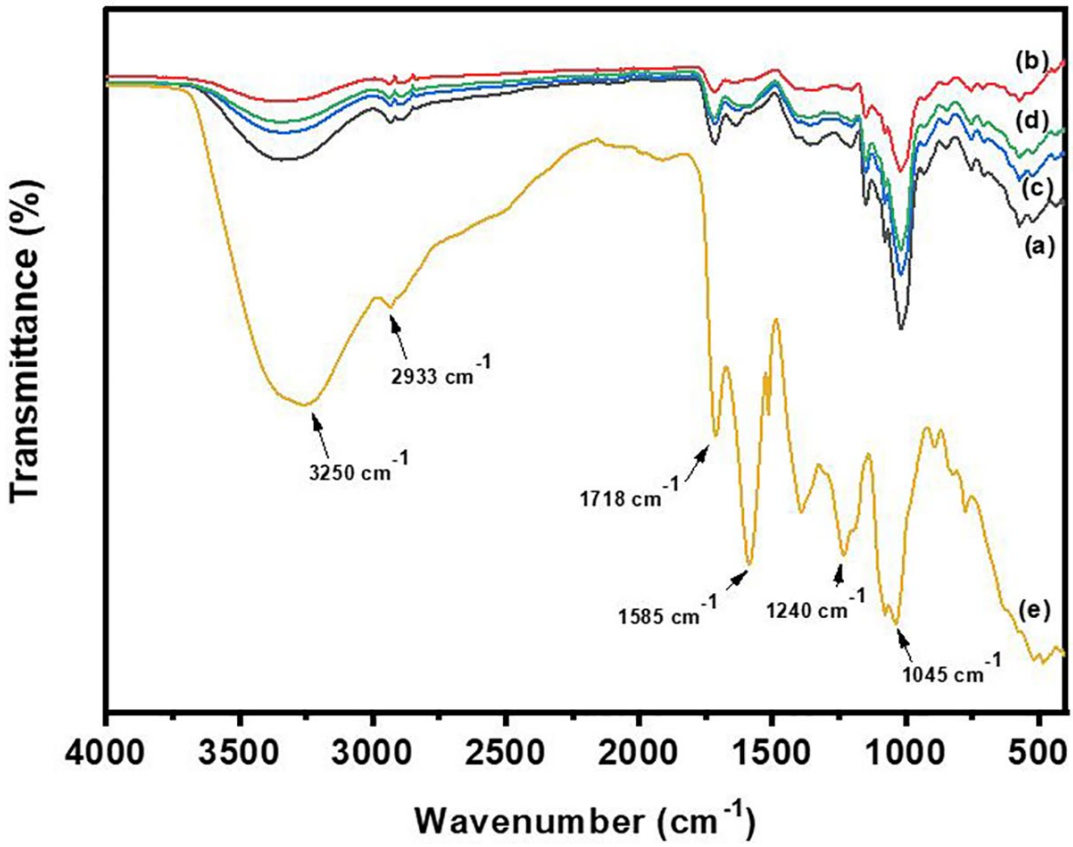

Figure 7. FTIR analysis on nanofibers: FTIR spectrum of nanofiber samples CH/PL (a), N1 (b), N50 (c), N100 (d), and dry N extract (e).

Water Absorption Capacity

Before submerging in DI water, an initial weight (W_i) measurement was recorded from a dry nanofiber sample. While submerged in DI water, the crosslinking membranes showed water stability while maintaining their nanofibrous structure. Samples were removed and air-dried, followed by a final weight (W_f) measurement. Through the water absorption capacity equation (Eq. 1), CH/PL and N100/CH/PL nanofibers were shown to have 377% and 442% water absorption capacity, respectively. Water absorption capabilities could be attributed due to hydrophilic characteristics of CH and PL (Xu *et al*., 2015), and to the N extract content which as previously described, the water absorption capacity of mucilage extract is due to a high structure of free hydroxyl groups (Bayar, Kriaa, & Kammoun, 2016; Rodriguez-Gonzalez *et al*., 2014); this was further confirmed through the swelling of the membranes after undergoing an N extract dip-coating process as shown in Figure 2(e). For tissue engineering purposes, an adequate absorption ability would be highly beneficial (Bacakova *et al*., 2004). This can be displayed in the ability of a nanofiber structure to merge with the ECM, allowing for cell migration, adhesion through fiber interaction, and promoting cell proliferation.

DMA

In Figure 8, mechanical analysis of DN100 before and after water absorption, a decrease in storage modulus (E') was demonstrated in the interval of analyzed temperature (23-40 °C). The initial measurements of E' at 23 °C were 87 and 42 MPa before and after water absorption, respectively. At low temperature, the stiffness of DN100 samples is expected given the crosslinking and brittleness of the dried samples. However, after water absorption, the sample regains its flexibility and quantitatively measured as a decrease in the storage modulus.

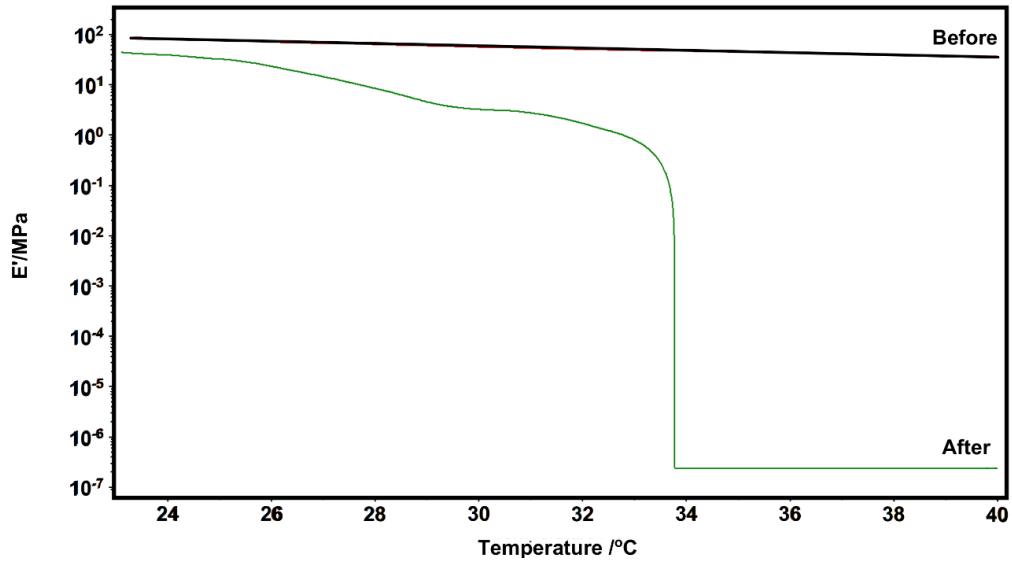

Figure 8. DMA of DN100 before and after a water absorption capacity test.

Bacterial Growth Study

For bacterial growth studies, nanofiber samples were incubated with inoculated *E. coli* to assay for their impact on bacterial growth. Sample inhibition zone measurements were determined by their diameter, where the absence of a clear zone was recorded as no inhibition. In Table 2, after 24 h CH/PL and N1 nanofiber membranes showed no signs of an inhibition zone, whereas N50 and N100 membranes exhibit a slight inhibition with a significant difference (*$p < 0.05$) compared to the control (Fig. 9(a-d)). The slight inhibition zones in N50 and N100 were still considered to have a bacterial resistance due to standard resistant measurements of *E. coli* against antibiotics (Hudzicki, 2009). This led to the approach of an N extract dip-coating process for antibacterial properties. Following dip-coating, SEM analysis of DN100 samples demonstrated a full coated layer and a change in fiber size due to uptake and retention of N extract, while sustaining the integrity of the material due to a heat mediated crosslinking (Fig. 10(a)). DN100 discs were laid onto agar plates with inoculated *E. coli* and incubated at 37 ºC. Further, a separate assessment of N extract was demonstrated, where crude N extract was loaded onto individual agar plates in the presence of inoculated *E. coli*. In Figure 10(b), after 24 h

DN100 showed total inhibition of bacterial growth, while crude N extract displayed similar inhibition of bacterial growth (Fig. 10(c)). Results were previously observed, where mature and immature *Opuntia* cladodes inhibited the growth of both *S. aureus* and *E. coli* (Blando *et al*., 2019; Suryawanshi & Vidyasagar, 2016). Further, *Opuntia* spp. mucilage contains phenolic acids, a range of 4-5 pH levels, leading to a bacterial susceptibility of membrane disruption, protein inactivation, and bacterial cell death (Khemiri, Hedi, Zouaoui, Gdara, & Bitri, 2019). The results that are shown in Figure 10(a-c), suggest that dip-coating confers both incorporated and outside inhibiting factors. In a supportive study, Texas sour orange juice (SOJ) dip-coating process allowed for the inhibition against *E. coli* and *S. aureus* bacteria, while demonstrating a structural integrity (Akia *et al*., 2019). Our results indicated that incorporation of N extract confers antibacterial properties, allowing a possible adequate environment for mammalian cell growth.

Table 2. Zone of Inhibition Analysis: A mean ±standard deviation (SD) diameter zone of inhibition measurement for CH/PL (control) was compared with N1, N50, and N100 against *E. coli*. (*p-value ≤ 0.05; (---) = no value) (n = 4 sample size).

Material on *E. coli*	**Sample Size**	**Inhibition Zone Mean±SD**	**P-value**
CH/PL	4	0±0	---
N1	4	0±0	> 0.05
N50	4	10.75±0.289	*< 0.05
N100	4	11.38±0.629	*< 0.05

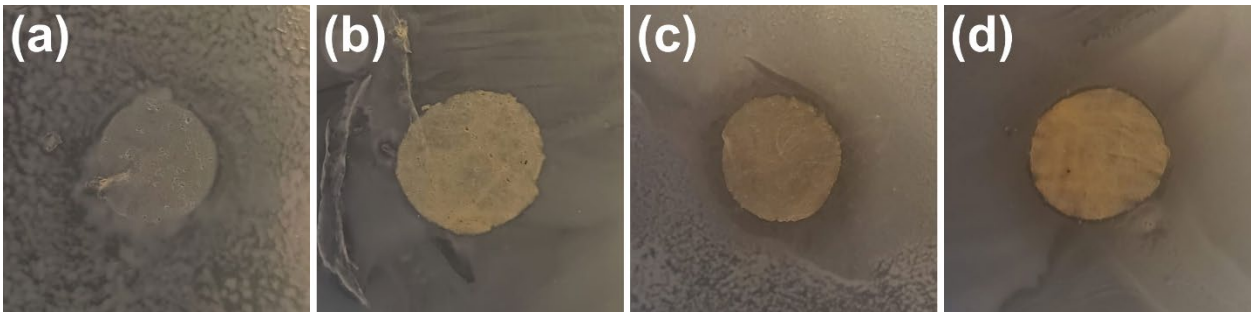

Figure 9. Images of Antibacterial Study: CH/PL (a), N1 (b), N50 (c), and N100 (d) nanofiber disks are displayed against *E. coli* on agar plates. (n = 4 sample size).

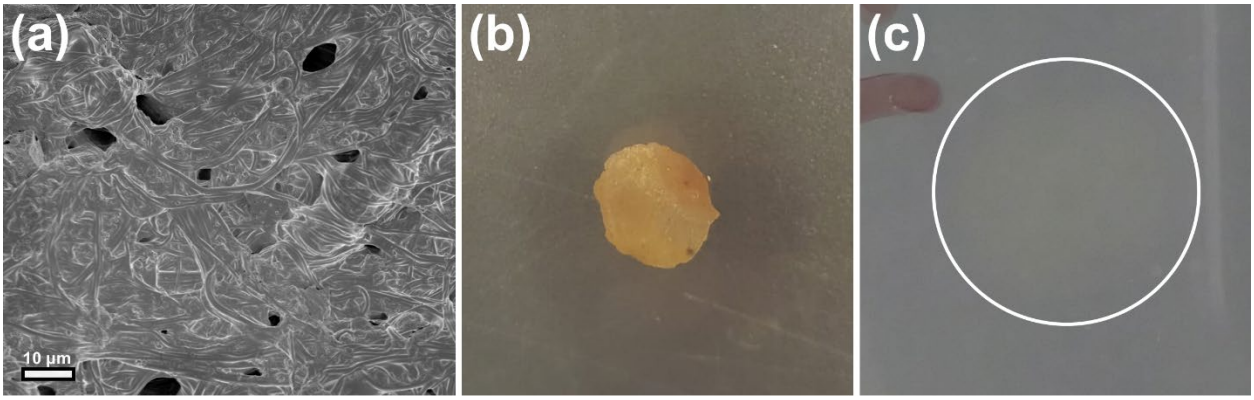

Figure 10. DN100 SEM Characterization and Bacterial Growth: Membrane morphology (a) and images from an antibacterial analysis of DN100 (b) compared to N extract (white circle) (c) are shown against *E. coli*. (SEM Mag. = 1.00 KX) (n = 4 sample size).

Cell Adhesion and Proliferation

To determine 3T3 cell localization and morphology within nanofibers, MitoTracerRed CMXRos (MTR) dye was used for staining the mitochondria and DAPI for cell nuclei. MTR is a rhodamine-derived dye that is taken up by organelles with an active mitochondrial transmembrane potential (Xu *et al*., 2015). Using confocal microscopy, representative images were captured using a grid scan method (Fig. 11), demonstrating cell presence throughout the sample area. Figure 12 shows the representative images of cell adhesion and proliferation presence onto nanofiber

samples after a 2, 4, and 6 day incubation period. After incubation, nanofiber samples were lifted and placed in a new 6-well dish to prevent the detection of non-adherent cells. Fluorescent treatment allowed for the localization of cells, where the staining of fibers was also exhibited due to possible hydrophilic property or dimers that allowed the retention or affinity of DAPI and MTR. Cell morphology in CH/PL samples appeared rounded throughout its nanofiber structure. Small-diameter pore size in the nanofiber matrix may reducing a migration capability due to a lack of penetration (Jenkins & Little, 2019). This compares to N50, N100, and DN100 nanofibers, where an elongated cell morphology is shown through MTR signaling. In a separate assessment of cell morphology, SEM micrographs of 3T3 cells were shown after a 6 day incubation period. Control CH/PL displayed rounded cell morphology, while N100 nanofibers displayed a more extended cellular morphology in the nanofiber matrix (Fig. 13), further demonstrating cell adhesion of N extract composite nanofibers.

Engineered materials can support cell growth onto fiber diameters around < 400 nm, promoting differentiation and beneficiary gene expression depending on the cell line, allowing the nanofibers to resemble the ECM (Jenkins & Little, 2019). As a supportive structure, the ECM promotes cell adhesion and proliferation. Nanofibrous structures can present similar characteristics for cell migration and alignment.

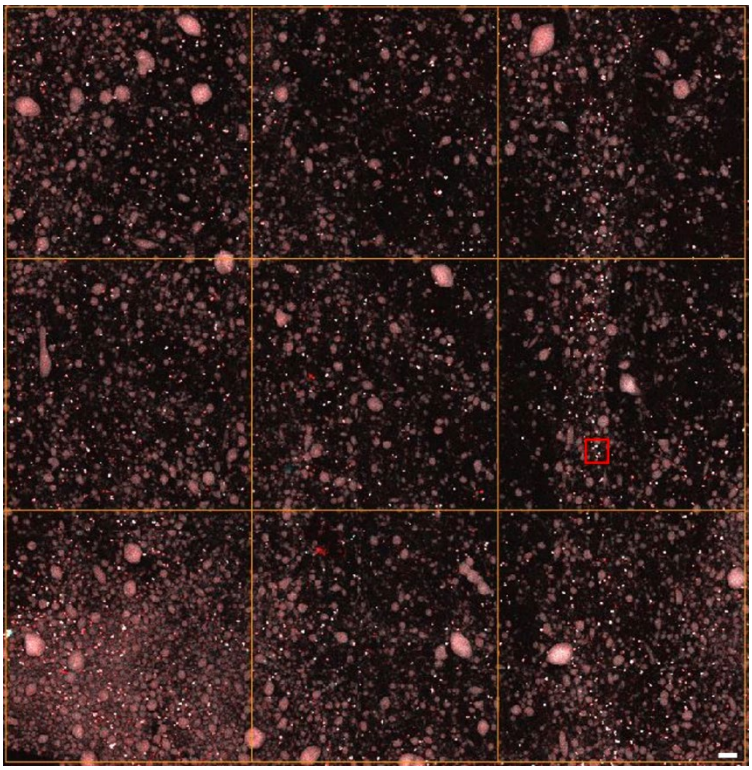

Figure 11. Representative Grid Map Image of Nanofiber Membrane Surface Area: Through confocal microscopy, a grid scan is used to capture 10 representative images for cell growth analysis. Selected image section (Red box) 212 x 212 μm. Scale bar = 200 μm.

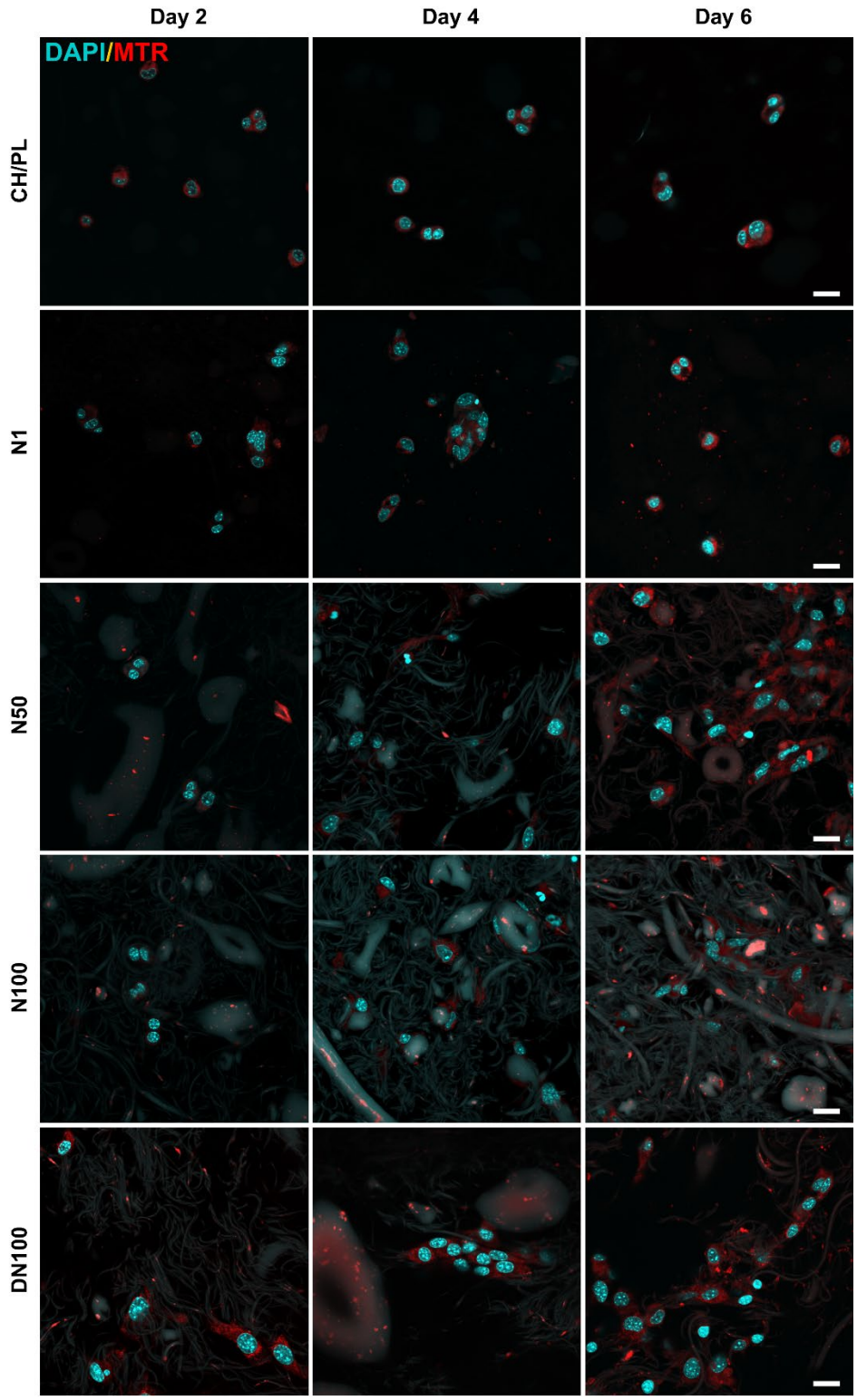

Figure 12. Confocal Microscopy of 3T3 Cell Adhesion and Proliferation on Nanofiber Membranes: 3T3 fibroblast cells were seeded onto nanofiber membranes in a 6-well dish and

treated after 2, 4, and 6 day incubation period. Cell adhesion was compared between control (CH/PL) with N1/CH/PL (N1), N50/CH/PL (N50), N100/CH/PL (N100), and N extract dip coated N100 (DN100) nanofibers. Samples were stained with DAPI (blue) for cell nuclei and MitoTracker Red for mitochondria. (n = 3 experiments). Scale bar = 20 μm. (60x magnification).

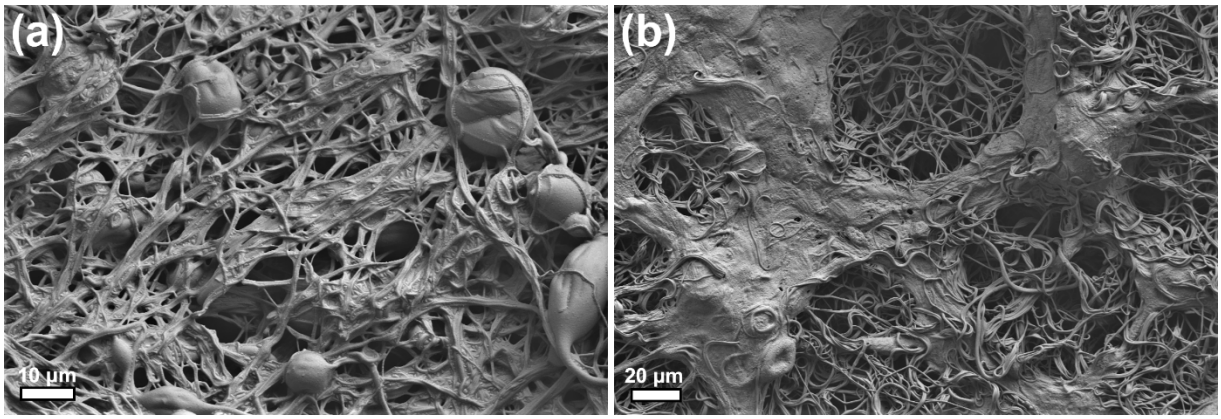

Figure 13. SEM 3T3 Cell Morphology: SEM micrographs are shown displaying 3T3 cell morphology onto control CH/PL (a) (scale bar = 10μm) and N100 (b) (scale bar = 20μm) nanofibers after a 6 day incubation. (n = 3 experiments).

After a 2 and 4-day incubation, cell adhesion and proliferation appear to be constant with no significant difference ($p > 0.05$) due to a standard error variation between most samples as by the average quantitative cell count method (Fig. 14). The only significant difference ($*p < 0.05$) was between N100 and DN100 on day 4 due to an initial slow cell progression with an N extract dip-coated layer. After a 6 day incubation period N50, N100, and DN100 composite nanofibers exhibited robust cell proliferation (Fig. 12); where a significant difference ($*p < 0.05$) in an average cell presence was shown in DN100 between the control and N1 (Fig. 14). An increase in DN100 cell proliferation could be based on a dip coating process, which over a 6-day incubation allowed for an improved cell culture media retention due to a water absorption capability (Monrroy *et al*., 2017; Ondarza, 2016). This further suggests that cell proliferation could be

attributed to the addition of the N extract and an adequate structure porosity (Cimmino *et al*., 2018) due to fiber diameter.

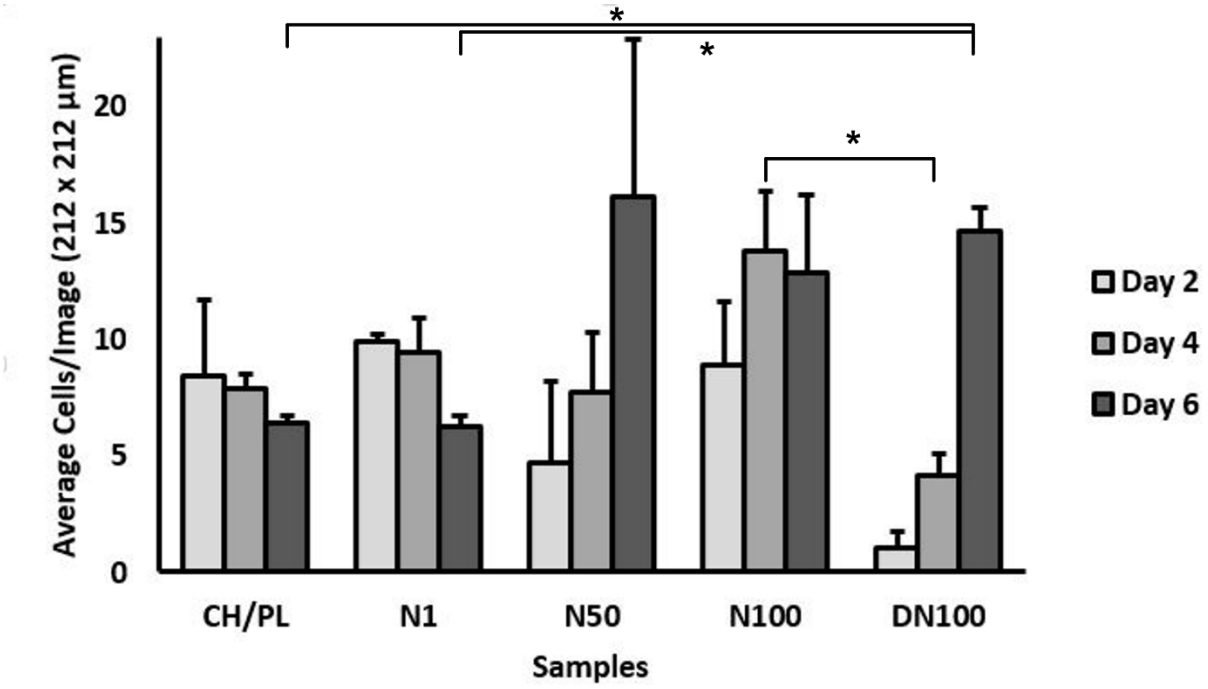

Figure 14. 3T3 Cell Average Presence/Image on Nanofibers: 3T3 cells were seeded onto nanofibers in a 6-well dish and treated after 2 day, 4 day, and 6 day incubation period. Cell proliferation was compared between control (CH/PL) with N1, N50, N100, and DN100 nanofibers. From a 3-trial experiment, an average cell presence/image was recorded from 10 images/sample. An ANOVA/Post-hoc Tukey statistical analysis is shown measuring the standard error of the mean +/- (SEM). (* P - value < 0.05).

Cell Viability

In Figure 15, a Resazurin cell viability test was conducted to further asses the viability of present adherent cells found on these nanofiber membranes. This bioassay monitors cellular metabolic activity based on the fluorescence of reduced form resorufin (Saenz *et al*., 2016). After day 2, samples were treated with reactive salt Resazurin, where no significant difference (p >

0.05) was shown between the positive control, CH/PL, and N100 composite nanofibers. After day 4, N100 nanofibers were shown with a 3% increase in absorbance with a significant difference (*$p < 0.05$) between positive control and CH/PL nanofibers. In day 6, N100 nanofibers exhibited a constant 3% increase compared to positive control and CH/PL, where no significant difference was shown due to a possible cell confluency with an exposed reaction. Based on the cell viability results, 3T3 fibroblasts retain full viability on nanofibers.

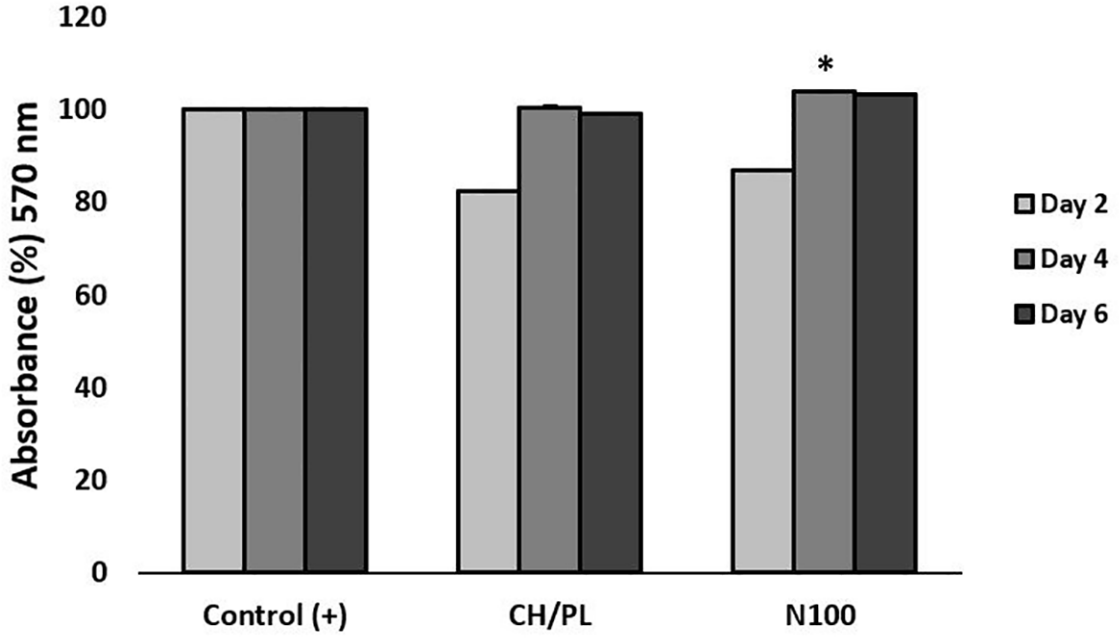

Figure 15. Resazurin Cell Viability Test: Cell viability was compared between control 3T3 cells on coverslip (Control (+)), CH/PL, and N100 nanofiber samples after a 2, 4, and 6 day incubation. An ANOVA/Post-hoc Tukey statistical analysis is shown with average sample absorbance (%) at 570 nm. (*P-value < 0.05). (n = 3 experiments).

3T3 Depth Analysis

To further observe cell proliferation and cell migration, a depth analysis was compared between control CH/PL and N100 composite nanofiber membranes after a 14 day incubation period. Figure 16(A, B) shows selected areas from the acquired nanofiber sample map images,

where a depth stepwise analysis was conducted with a series of 5 μm depth distance between every focal plane (Fig. 16(a, b)). A clear distinction in cell morphology and a representation of cell migration can be seen in both nanofiber samples. Control CH/PL nanofibers consistently showed a rounded cell morphology (Fig. 16(a)), where a lack of physical or chemical interaction could be observed due to a weak static or high hydroxyl bond that alters the cell adherence by cell adhesion molecules (CAMs) preventing any substrate adsorption capability (Bacakova, Filova, Rypacek, Svorcik, & Stary, 2004; Hoshiba, Yoshikawa, & Sakakibara, 2018; Takeichi & Okada, 1972). 3T3 cells can be observed to have a higher interaction within N100 composite nanofibers, as shown anchoring through an overlapping cell presence at different depths of the nanofibrous membrane. This can be seen through a Resazurin cell viability test, where a higher metabolic activity was shown due to cells adhering onto and migrating within N100 composite nanofibers, as described in a previous study where a nanofiber structure sustains the viability of migrating cells (Dashdorj *et al*., 2015). Our results suggest that after 14 days, cell adhesion and proliferation are consistent with favorable environment in N100 composite nanofibers.

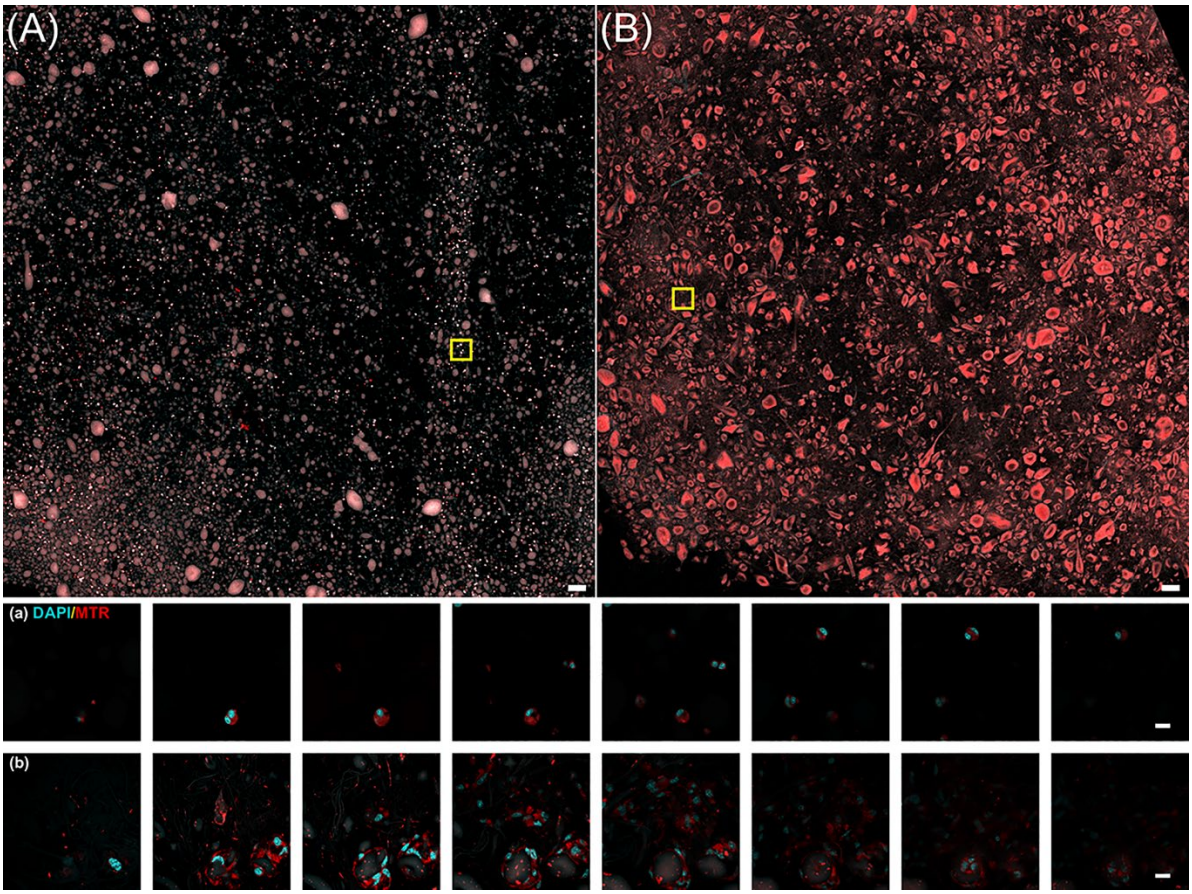

Figure 16. Depth Analysis of CH/PL and N100 Nanofibers: Confocal microscopy of CH/PL (A) and N100 (B) nanofiber sample map images are shown, with a selected image section (yellow box) 212 x 212 µm. Scale bar = 200 µm. A depth analysis was compared after a 14 day incubation period between control (CH/PL) (a) and N100 (b) nanofibers, where a stepwise analysis was conducted with a series of 5 µm depth distance between every focal plane. Scale bar = 20 µm. 60x magnification. (n = 3 experiments)

CHAPTER IV

SUMMARY AND CONCLUSION

Here, we show the successful incorporation of N extract into Forcespinning® composite nanofibers, with fiber matrix characteristics resembling an extracellular matrix (ECM) environment. In addition to characterizing the mechanical properties of these fibers, N/CH/PL composed nanofibers have antibacterial properties, while sustaining its nanofiber structure due to a crosslinking treatment. NIH 3T3 fibroblasts demonstrated robust cell adhesion and proliferation, while embracing an active non-toxic cellular activity. With an abundant crude *O. cochenillifera* extract incorporation, a nanofibrous membrane may confer an adsorption property enabling cell interconnectivity, allowing a promising wound repair and reepithelization of skin tissue. Further indicating the potential use of N/CH/PL composed nanofibers for wound healing applications, and the advancement in material sciences within other nanotechnology industries.

REFERENCES

Abbas, O., Compere, G., Lorondelle, Y., Pompeu, D., Rogez, H., Baeten, V. (2017). Phenolic compound explorer: A mid-infrared spectroscopy database. *Vibrational Spectroscopy*, 92, 111-118.

Ahn, S., Ardona, H. A. M., Campbell, P. H., Gonzalez, G. M., & Parker, K. K. (2019). Alfalfa Nanofibers for Dermal Wound Healing. ACS Appl. Mater. Interfaces, 11: 33535-3357. Doi: 10.1021/acsami.9b07626

Akia, M., Rodriguez, C., Materon, L., Gilkerson, R., Lozano, K. (2019). Antibacterial activity of polymeric nanofiber membranes impregnated with Texas sour orange juice. *European Polymer Journal*, 115, 1-5.

Akia, M., Salinas, N., Rodriguez, C., Gilkerson, R., Materon, L., Lozano, K. (2018). Texas Sour Orange Juice used in Scaffolds for Tissue Engineering. *Membranes*, 8(3): 38.

Andolfo, G., & Ercolano, M. R. (2015). Plant Innate Immunity Multicomponent Model. *Font. Plant Sci.* 6:987. Doi: 10.3389/fpls.2015.00987

Attanzio, A., Frazzitta, A., Busa, R., Tesoriere, L., Livrea, M. A., & Allegra, M. (2019). Indicaxanthin from *Opuntia ficus indica* (L. Mill) Inhibits Oxidized LDL-Mediated Human Endothelial Cell Dysfunction through Inhibition of NF-kB Activation. *Oxidative Medicine and Cellular Longevity*. https://doi.org/10.1155/2019/345846

Bacakova, L, Filova E, Rypacek F, Svorcik V, Stary V. (2004). Cell Adhesion on Artificial Materials for Tissue Engineering. *Physiol. Res*, 53(SUPPL.1), S35-S45.

Bayar N, Kriaa M, Kammoun R. (2016). Extraction and characterization of three polysaccharides extracted from Opuntia ficus indica cladodes. *International Journal of Biological Macromolecules*, 92, 441-450.

Blando, F., Russo, R., Negro, C., De Bellis, L., Frassinetti, S. (2019). Antimicrobial and Antibiofilm Activity against Staphylococcus aureus of Opuntia ficus-indica (L.) Mill. Cladode Polyphenolic Extracts. *Antioxidants*, 8(5): 117. Doi: 10.3390/antiox8050117.

Boller, T., & He S. Y. (2009). Innate immunity in plants: An arms race between pattern recognition receptors in plants and effectors in microbial pathogens. *Science*. 324(5928): 742-744. Doi: 10.1126/science.1171647

Boyle, W., Chen, W., Rodriguez, A., Linn, S., Tolar, J., Lozano, K., Reineke, T. (2019). Ternary Composite Nanofibers Containing Chondroitin Sulfate Scavenge Inflammatory Chemokines from Solution and Prohibit Squamous Cell Carcinoma Migration. *ACS Appl. Bio Mater*, 2(2), 619-624.

Calil, I. P., & Fontes, E. P. B. (2017). Plant immunity against viruses: antiviral immune receptors in focus. *Annals of Botany*. 119: 711-723. Doi: 10.1093/aob/mcw200

Cardenas, A., Higuera-Ciapara, I., Goycoolea, F. (1997). Rheology and Aggregation of Cactus (Opuntia ficus-indica) Mucilage in Solution. *J. PACD*, 2, 152-159.

Chau, B. N., Chen, T., Wan, Y. Y., DeGregori, J., Wang, J. Y. J. (2004). Tumor Necrosis Factor Alpha-Induced Apoptosis Requires p73 and c-ABL Activation Downstream of RB Degradation. *MCB*. Vol. 24, No. 10, p. 4438-4447.

Chen, L., Yan, C., Zheng, Z. (2018). Functional polymer surfaces for controlling cell behaviors. *Materials Today*, 21(1): 38-59. https://doi.org/1016/j.mattod.2017.07.002

Chen, S., Sun, M., Wang, B., Hao, L., Zhang, C., Xin, Y. (2011). Wound healing effects of cactus extracts on second degree superficial burn mice. *Journal of Medicinal Plants Research*, 5(6), 973-978.

Cimmino, C., Rossano, L., Netti, P. A., and Ventre, M. (2018). Spatio-Temporal Control of Cell Adhesion: Toward Programmable Platforms to Manipulate Cell Functions and Fate. *Bioeng. Biotechnol*, 6, 190. Doi: 10.3389/fbioe.2018.00190

Coltelli M, Danti S, De Clerk K, Lazzeri A, and Morganti P. (2020). Pullulan for Advanced Sustainable Body- and Skin-Contact Applications. *J Funct. Biomater*, 11(20): 1-17.

Cremar, L., Gutierrez, J., Martinez, J., Materon, L., Gilkerson, R., Xu, F., Lozano, K. (2018). Development of antimicrobial chitosan based nanofiber dressings for wound healing applications. *Nanomed. J*., 5(1), 6-14. Doi: 10.22038/nmj.2018.05.002

Da Cruz Filho I. J., et al. (2019). Lignins isolated from Prickly pear cladodes of the species Opuntia ficus-indica (Linnaeus) Miller and Opuntia cochenillifera (Linnaeus) Miller induces mice splenocytes activation, proliferation and cytokines production. *International Journal of Biological Macromolecules*, 123, 1331-1339. https://doi.org/10.1016/j.ijbiomac.2018.09.120

Dashdorj, U., Reyes, M., Unnithan, A., Tiwari, A., Tumurbaatar, B., Park, C., Kim, C. (2015). Fabrication and characterization of electrospun zein/Ag nanocomposite mats for wound dressing applications. *International Journal of Biological Macromolecules*, vol. 80, 1-7.

De J. Cano-Barrita P.F. & Leon-Martinez F. M. (2016). Biopolymers with viscosity-enhancing properties for concrete. *Biopolymers and Biotech Admixtures for Eco-Efficient Construction Materials*. http://dx.doi.org/10.1016/B978-0-08-100214-8.00011-7

DeClue, C. E., Shornick, L. P. (2015). The cytokine milieu of diabetic wounds. *Diabetes Manag*. 5(6), 525-537.

Del Socorro Santos Diaz, M., Barba De la Rosa, A.P., Helies-Toussaint, C., Gueraud, F., Negre-Salvayre, A. (2017). Opuntia spp.: Characterization and Benefits in Chronic Diseases. *Oxidative Medicine and Cellular Longevity*, vol. 2017: 17. Doi: 10.1155/2017/8634249

El-Mostafa, K., El Kharrassi, Y. Badreddine, A., Andreoletti, P., Vamecq, J., El Kebbaj, M., Latruffe, N., Lizard, G., Nasser, B., & Cherkaoui-Malki, M. (2014). Nopal Cactus (Opuntia ficus-indica) as a Source of Bioactive Compounds for Nutrition, Health and Disease. *Molecules*, 19(9), 14879-14901. Doi: 10.3390/molecules190914879.

Golkar P., Allafchian A., Afshar B. (2018). *Alyssum lepidium* mucilage as a new source for electrospinning: production and physicochemical characterisation. *IET Nanobiotechnol*, 12(3): 259-263. Doi: 10.1049/iet-nbt.2017.0133

Gouveia, B. C., Calil, I. P., Machado, J. P. B., Santos, A. A., Fontes, E. P. B. (2017). Immune Receptors and Co-receptors in Antiviral Innate Immunity in Plants. *Front. Microbial*. 7:21939. Doi: 10.3389/fmicb.2016.02139

Guadarrama-Lezama, A. Y., Castaño, J., Velazquez, G., Carillo-Navas, H., & Alvarez-Ramirez, J. (2018). Effect of Nopal mucilage Addition on Physical, Barrier and Mechanical Properties of Citric Pectin-Based Films. *Journal of Food Science and Technology*, 55(9), 3739-3748.

Guo, S., & Di Pietro, L. (2010). Critical Review in oral biology & medicine: Factors Affecting Wound Healing. *J Dent Res*, 89(3), 219-229. Doi: 10.1177/0022034509359125

Hajialyani, M., Tewari, D., Sobarzo-Sanchez, E., Nabavi, S. M., Farzaei, M. H., Abdollahi, M. (2018). Natural product-based nanomedicines for wound healing purposes: Therapeutic targets and drug delivery systems. *International Journal of Nanomedicine*, 13, 5023-5043.

Harth, K. C., Rosen, M. J. (2009). Major complications associated with xenograft biologic mesh implantation in abdominal wall reconstruction. *Surgical Innovation*, (4): 324-9.

Hernandez-Carillo, C., Gomez-Cuaspud, J., & Martinez-Suarez, C. (2017). Composition, thermal and microstructural characterization of the Nopal (opuntia ficus inidica), for addition in commercial cement mixtures. *J. Phys.: Conf. Ser*., 935(1). Doi: 10.1088/1742-6596/935/1/012045

Hoshiba T., Yoshikawa C., & Sakakibara K. (2018). Characterization of Initial Cell Adhesion on Charged Polymer Substrates in Serum-Containing and Serum-Free Media. *Langmuir*, 34, 4043-4051. Doi: 10.1021/acs.langmuir.8b0023

Hudzicki, J. (2009). Kirby-Bauer Disk Diffusion Susceptibility Test Protocol. *American Society for Microbiology*, (December 2009), 1-14.

http://scholar.google.com/sholar?hl=en&btnG=Search&q=intitle:Kirby-Bauer+Disk+Diffusion+Suceptibility+Test+Protocol#0

Jenkins, T. L., Little, D. (2019). Synthetic scaffolds for musculoskeletal tissue engineering cellular responses to fiber parameters. *npj Regen Med*, vol. 4, 15. https://doi.org/10.1038/s41536-019-0076-5

Karim, M., Lee, H., Kim, R., Ji, B., Cho, J., Son, T., Oh, W., Yeum, J. (2009). Preparation and characterization of electrospun pullulan/montmorillonite nanofiber mats in aqueous solution. *Carbohydrate Polymers*, 78(2), 336-342.

Keen, M. A., Hassan, I. (2016). Vitamin E in dermatology. *Indian Dermatol Online J*, 7, 311-5.

Khemiri, I., Essghaier Hedi, B., Sadfi Zouaoui, N., Ben Gdara, N., Bitri, L. (2019). The Antimicrobial and Wound Healing Potential of Opuntia ficus indica L. inermis Extracted Oil from Tunisia. *Evidence-based Complementary and Alternative Medicine*, 2019(12): 1-10. http://doi.org/10.1155/2019/9148782.

Kiesling, R. (1995). Origen, Domesticacion y Distribucion de Opuntia ficus-indica. *J. Profess. Assoc. Cact. Develop*, Vol. 22(1642), 4747-4748.

Kumar, N., & Goel, N. (2019). Phenolic acid: Natural versatile molecules with promising therapeutic applications. *Biotechnology reports*, 24: 1-10. https://doi.org/10.1016/j.btre.2019.e00370

Kushalappa, A. C., Yogendra, K. N., & Karre, S. (2016). Plant Innate Immune Response: Qualitative and Quantitative Resistance. *Critical Reviews in Plant Sciences*, 35(1): 38-55. Doi: 10.1080/07352689.2016.1148980

Lanuzza, F., Occhiuto, F., Monforte, M. T., Tripodo, M. M., D'Angelo, Galati, E. M. (2017). Antioxidant phytochemicals of Opuntia ficus-indica (L.) Mill. cladodes with potential anti-spasmodic activity. *Phcog Mag*, 13, S424-9. Doi: 10.4103/pm_495_16

Lee, J., Kim, H., Kim, J., & Jang, Y. (2002). Antioxidant Property of an Ethanol Extract of the Stem of Opuntia ficus-indica var. Saboten. *J. Agric. Food Chem*., Vol. 50, 6490-6496.

Lobo, V., Patil, A., Phatak, A., & Chandra, N. (2010). Free radicals, antioxidants and functional foods: Impact on human health. *Pharmacogn Rev*., 4(8), 118-126. Doi: 10.4103/0973-7847.70902

Lopez-Garcia, F., Jimenez-Martinez, C., Guzman-Lucero, D., Maciel-Cerda, A., Delgado-Macuil, R., Cabrero-Palomino, D., Terres-Rojas, E., Arzate-Vazquez, I. (2017). Physical and Chemical Characterization of a Biopolymer Film made with Corn Starch and *Nopal Xoconostle*. *Revista Mexicana de Ingenieria Quimica*, 16(1), 147-158.

Lunni, D., Cianchetti, M., Filippeschi, C., Sinibaldi, E., & Mazzolai, B. (2020). Plant-Inspired Soft Bistable Structures Based on Hygroscopic Electrospun nanofibers. *Adv. Mater. Interfaces*, 7: 1-8. Doi: 10.1002/admi.201901310

MacLeod, A. S., & Mansbridge, J. N. (2014). The Innate Immune System in Acute and Chronic Wounds. *ADCANCES IN WOUND CARE*. 5(2): 65-78. Doi: 10.1089/wound.2014.0608

Malik, N. A. A., Kumar, I. S., & Nadarajah, K. (2020). Elicitor and Receptor Molecules: Orchestrators of Plant Defense and Immunity. *Int. J. Mol. Sci*. 21(963). Doi: 10.3390/ijms21030963

Mohammed, M. H., Taiseer Hassan, M., Youssif, A. A. A. (2019). Production of Fiber From Mesquite Plant (prosopis juliflora. L.). *IJEAS*, 6(9). ISSN: 2394-3661.

Majure, L. & Puente, R. (2014). Phylogenetic relationships and morphological evolution in Opuntia s.str. and closely related members of tribe Opuntieae. *Succulent Plant Research*, vol. 8(January), 9-30.

Monrroy, M., Garcia, E., Rios, K., Garcia, J. (2017). Extraction and Physicochemical Characterization of Mucilage from Opuntia cochenillifera (L.) Miller. *Journal of Chemistry*, vol. 2017: 9. https://doi.org/10.1155/2017/4301901

Nady, N., & Kandil, S.H. (2018). Novel blend for producing porous chitosan-based films suitable for biomedical applications. *Membranes*, 8(1): 2. https://doi.org/10.3390/membranes8010002

Nishad, R., Ashmed, T., Rahman, V. J., & Kareem, A. (2020). Modulation of Plant Defense System in Response to Microbial Interactions. *Front. Microbiol*. 11:1298. Doi: 10.3389/fmicb.2020.01298

Obregon, N., Agubra, V., Pokhrei, M., Campos, H., Flores, D., De la Garza, D., Mao, Y., Macossay, J., & Alcoutlabi, M. (2016). Effect of Polymer Concentration, Rotation Speed, and Solvent Mixture on Fiber Formation Using Forcespinning®. *Fibers*, 4, 20. Doi: 10.3390/fib4020020

Olivarez-Perez, A., Toxqui-Lopez, S., & Padilla-Velasco, A. (2012). Nopal Cactus (Opuntia Ficus-Indica) as a Holographic Material. *Materials*, 5(11), 2383-2402.

Ondarza, M. (2016). Cactus Mucilage: Nutritional, Health Benefits and Clinical Trials. *Journal of Medical and Biological Science Research*, vol. 2(6), 87-103.

Osuna-Martinez, L., Reyez-Esparsa, J., & Rodriguez-Fragoso, L. (2014). Cactus (Opuntia ficus-indica): A Review on its Antioxidants Properties and Potential Pharmacological Use in Chronic Diseases. *Nat Prod Chem Res*, 2(6): 153-160. Doi:10.4172/2329-6836.1000153

Padilla-Gainza, V., Morales, G., Rodriguez-Tobias, H., Lozano, K. (2019). Forcespinning technique for the production of poly(d,1-lactic acid) submicrometer fibers: Process-morphology-properties relationship. *Journal of Applied Polymer Science*, 136(22), 1-9.

Padilla-Gainza, V., Rodriguez-Tobias, H., Morales, G., Ledezma-Perez, A., Alvarado-Canche, C., Rodriguez, C., Robert, G., & Lozano, K. (2020). Processing-structure-property relationships of biopolyester/zinc oxide fibrous scaffolds engineered by centrifugal spinning. *Polym Adv Technol*. 1-14. https://doi.org/10.1002/pat.4987

Padron, S., Fuentes, A., Caruntu, D., Lozano, K. (2013). Experimental study of nanofiber production through forcespinning. *Journal Applied Physics*, 113(2). https://doi.org/10.1063/1.4769886

Pais, Y. (2011). Fabrication and Characterization of Electrospun Cactus Mucilage Nanofibers. *Graduate Theses and Dissertations*, 46. http://scholarcommons.usf.edu/etd/3279

Park, S. N. (2002). Cacti: Biology and Uses. *University of California Press*. 222-245, ill., index. ISBN: 0-520-23157-0.

Parameswaran, N., Patial, S. 2010. Tumor Necrosis Factor-α Signaling in Macrophages. *Crit Rev Eukaryot Gene Expr*. 20(2):87-103.

Patel, K. N., & Ishnava, K. B. (2018). Evaluation of Nutritional and Medicinal Properties of Opuntia elatior Mill. *Phytochemicals-Source of Antioxidants and Role in Disease Prevention*, 121-138. http://dx.doi.org/10.5772/intechopen.77081

Pelissari, F. M., Andrade-Mahecha, M. M., Sobral, P. J. do A., Menegalli, F. C. (2017). Nanocomposites based on banana starch reinforced with cellulose nanofibers isolated from banana peels. *Journal of Colloid and Interface Science*, 505: 154-167. http://dx.doi.org/10.1016/j.jcis.2017.05.106

Pereira R. F., Carvalho A., Gil M. H., Mendes A., Bartolo P. J. (2013). Influence of *Aloe vera* on water absorption and enzymatic *in vitro* degradation of alginate hydrogel films. *Carbohydrate Polymers*, 98: 311-320. http://dx.doi.org/10.1016/j.carbpol.2013.05.076

Ranjbar-Mohammad M., Bahrami S. H., Joghataei M. T. (2013). Fabrication of novel nanofiber scaffolds from gum tragacanth/poly(vinyl alcohol) for wound dressing application: In vitro evaluation and antibacterial properties. *Materials Science and Engineering C*, 33: 4935-4943. https://doi.org/10.1016/j.msec.2013.08.016

Riss, T. L., Moravec, R. A., Niles, A. L., Duellman, S., Benink, H. A., Worzella, T. J., & Minor, L. (2016). Cell Viability Assays (Promega). *Assay Guidance Manual*, 7-11. URL: https://www.ncbi.nlm.nih.gov/books/NBK144065/

Rodriguez-Gonzalez, S., Martinezz-Flores, H., Chavez-Moreno, C., Macias-Rodriguez, L., Zavala-Mendoza, E., Garnica-Romo, M., Chacon-Garcia, L. (2014). Extraction and

characterization of mucilage from wild species of Opuntia. *Journal of Food Process Engineering*, 37(3): 285-292 (2014). Doi:10.1111/jfpe.12084

Saenz, C., Sepulveda, E., Matsuhiro, B. (2004). Opuntia spp mucilage's: a functional component with industrial perspectives. *Journal of Arid Environments*, 57(3), 275-290.

Salmon, T., Evert, B., Song, B., Doetsh, P. (2004). Biological consequences of oxidative stress-induced DNA damage in Saccharomyces cerevisiae. *Nucleic Acids Research*, vol. 32(12), 3712-3723. Doi:10.1093/nar/gkh696

Sen, C. K. (2019). Human Wounds and Its Burden: An Update Compendium of Estimates. *ADVANCES IN WOUND CARE*, 8(2): 39-51. Doi: 10.1089/wound.2019.0946

Sepulveda, E., Saenz, C., Aliaga, E., Aceituno, C. (2007). Extraction and characterization of mucilage in Opuntia spp. *Journal of Arid Environments*, 68(4), 534-545. Doi:10.1016/j.jaridenv.2006.08.001

Sherwood, L. (2016). Human physiology from cells to systems Ninth Edition. *Appetite*, vol. 20, issue 3, 404-442.

Shi, R., Bi, J., Zhang, Z., Zhu, A., Chen, D., Zhou, X., Zhang, L., Tian, W. (2008). The effect of citric acid on the structural properties and cytotoxicity of the polyvinyl alcohol/starch films when molding at high temperature. *Carbohydrate Polymers*, 74(4), 763-770. Doi:10.1016/j.carbpol.2008.04.045

Sitarek, P., Merecz-Sadowska, A., Kowalczyk, T., Wieczfinska, J., Zajdel, R., & Sliwinski, T. (2020). Potential Synergistic Action of Bioactive Compounds from Plant Extracts against Skin Infection Microorganisms. *Int. J. Mol. Sci.*, 21, 5105. Doi: 10.3390/ijms21145105

Stintzing, F., & Carle, R. (2005). Cactus stems (Opuntia spp.): A review on their chemistry, technology, and uses. *Mol. Nutr. Food Res*, 49(2), 175-194 (2005). Doi: 10.1002/mnfr.200400071

Suryawanshi, P., & Vidyasagar, G. (2016). Antimicrobial Activity of Opuntia cochenillifera (L.) Mill Fruit and Cladode Extracts. *International Journal of Pharmacology, Phytochemistry and Ethnomedicine*, vol. 3, 84-89.

Takeichi M. & Okada T. S. (1972). Roles of Magnesium and Calcium Ions In Cell-To-Substrate Adhesion. *Experimental Cell Research*, 74, 51-60.

Tanaka, T., Narazaki, M., Kishimoto, T. (2014). IL-6 In Inflammation, Immunity, and Disease. *Cold Spring Harb Perspect Biol*. 4;6.

Teixeira, M. d. C., Santini, A, & Souto, E. B. (2017). Chapter 8: Delivery of Antimicrobial by Chitosan-Composed Therapeutic Nanostructures. *Nanostructures for Antimicrobial Therapy*, 203-222. https://doi.org/10.1016/B978-0-323-46152-8.00008-1

Thomas, S., & Alcantar, N. (2017). System integration of functionalized natural materials. *MRS Bulletin*, Vol. 42(5), 343-349. https://doi.org/10.1557/mrs.2017.90

Urena-Saborio, H., Alfaro-Viquez, E., Esquival-Alvarado, D., Madrigal-Carballo, S., Gunasekaran, S. (2018). Electrospun plant mucilage nanofibers as biocompatible scaffolds for cell proliferation. *International Journal of Biological Macromolecules*. 115: 1218-1224. https://doi.org/10.1016/j.ijbiomac.2018.04.129

Vieyra H., Figueroa-Lopez U., Guevara-Morales A., Vergara-Porras B., San Martin-Martinez E., and Aguilar-Mendez A. (2015). Optimized Monitoring of Production of Cellulose Nanowhiskers from *Opuntia ficus-indica* (Nopal Cactus). *International Journal of Polymer Science*, 1-8. http://dx.doi.org/10.1155/2015/871345

Xu, F., Weng, B., Gilkerson, R., Materon, L., Lozano, K. (2015). Development of tannic acid/chitosan/pullulan composite nanofibers from aqueous solution for potential applications as wound dressing. *Carbohydrate Polymers*, 115, 16-24.

Xu, F., Weng, B., Materon, L., Gilkerson, R., Lozano, K. (2014). Large-scale production of a ternary composite nanofiber membrane for wound dressing applications. *Journal of Bioactive and Compatible Polymers*, 29(6): 646-660.

Xu, F., Zhang, C., and Graves, D. T. (2013). Abnormal Cell Response and Role of TNF-α in Impaired Diabetic Wound Healing. *BioMed Research International*. Pgs. 9.

Yasmeen, S., Kabiraz, M., Saha, B., Qadir, M., Gafur, M., & Masum, S. (2016). Chromium (VI) Ions Removal from Tannery Effluent Using Chitosan-Microcrystalline Cellulose Composite as Adsorbent. *International Research Journal of Pure and Applied Chemistry*, 10(4), 1-14. Doi: 10.9734/IRJPAC/2016/23315

Zhang, W., Ronca, S., & Mele, E. (2017). Electrospun Nanofibres Containing Antimicrobial Plant Extracts. *Nanomaterials*. 7(42). Doi: 10.3390/nano7020042

Zhuang, L., Zhi, X., Du, B., & Yuan, S. (2020). Preparation of Elastic and Antibacterial Chitosan- Citric Membranes with High Oxygen Barrier Ability by in Situ Cross-Linking. *ACS Omega*, 5(2), 1086-1097. https://doi.org/10.1021/acsomega.9b03206

BIOGRAPHICAL SKETCH

Cristobal Rodriguez, completed his Bachelor of Fine Arts in Art, at The University of Texas Rio Grande Valley Fall of 2019. During which he spend conducting research within an interdisciplinary focus between biology and engineering through the Partnership for Research and Education in Materials Science (PREM) program. Then proceeded in completing a Master of Science in Biology at the University of Texas Rio Grande Valley in Spring 2021. Contact information, e-mail: cristobal.rodriguez01@utrgv.edu.